Northern Hemisphere atmospheric history of carbon monoxide since preindustrial times reconstructed from multiple Greenland ice cores

Xavier Faïn[1], Rachael H. Rhodes[2], Philip Place[3], Vasilii V. Petrenko[3], Kévin Fourteau[4],
Nathan Chellman[5], Edward Crosier[3], Joseph R. McConnell[5], Edward J. Brook[6], Thomas Blunier[7],
Michel Legrand[8], and Jérôme Chappellaz[1]

[1]Univ. Grenoble Alpes, CNRS, IRD, Grenoble INP, IGE, 38000 Grenoble, France
[2]Department of Earth Sciences, University of Cambridge, Cambridge, CB2 3EQ, UK
[3]Department of Earth and Environmental Sciences, University of Rochester, Rochester, NY, USA
[4]Univ. Grenoble Alpes, Université de Toulouse, Météo-France, CNRS, CNRM, Centre d'Études de la Neige, Grenoble, France
[5]Division of Hydrologic Sciences, Desert Research Institute, Reno, NV 89512, USA
[6]College of Earth, Ocean, and Atmospheric Sciences, Oregon State University, Corvallis, OR 97331, USA
[7]Centre for Ice and Climate, Niels Bohr Institute, University of Copenhagen, Copenhagen, Denmark
[8]LISA, UMR CNRS 7583, Université Paris-Est Créteil, Université de Paris, Institut Pierre Simon Laplace (IPSL), Créteil, France

Correspondence: Xavier Faïn (xavier.fain@univ-grenoble-alpes.fr)

Abstract. Carbon monoxide (CO) is a regulated pollutant and one of the key components determining the oxidizing capacity of the atmosphere. Obtaining a reliable record of atmospheric CO mixing ratios since pre-industrial times is necessary to evaluate climate-chemistry models in conditions different from today and to constrain past CO sources. We present high-resolution measurements of CO mixing ratios from ice cores drilled at five different sites on the Greenland ice sheet which experience a range of snow accumulation rates, mean surface temperatures, and different chemical compositions. An optical-feedback cavity-enhanced absorption spectrometer (OF-CEAS) was coupled to continuous melter systems and operated during four analytical campaigns conducted between 2013 and 2019. Overall, continuous flow analyses (CFA) of CO were carried out on over 700 m of ice. The CFA-based CO measurements exhibit excellent external precision (ranging 3.3-6.6 ppbv, 1σ), and achieve consistently low blanks (ranging from 4.1 ± 1.2 to 12.6 ± 4.4 ppbv), enabling paleo-atmospheric interpretations. However the five CO records all exhibit variability too large and rapid to reflect past atmospheric mixing ratio changes. Complementary tests conducted on discrete ice samples demonstrate that these variations are not artifacts of the analytical method (i.e., production of CO from organics in the ice during melting), but very likely are related to in situ CO production within the ice before analysis. Evaluation of signal resolution and co-investigation of high-resolution records of CO and TOC suggest that past atmospheric CO variations can be extracted from the records' baselines with accumulation rates higher than 20 cm water equivalent per year (weq yr^{-1}). Consistent baseline CO records from four Greenland sites are combined to produce a multisite average ice core reconstruction of past atmospheric CO for the Northern Hemisphere high latitudes, covering the period from 1700 to 1957 CE. Such reconstruction should be taken as an upper bound of past atmospheric CO abundance. From 1700 to 1875 CE, the record reveals stable or slightly increasing values in the 100-115 ppbv range. From 1875 to 1957 CE, the record indicates a monotonic increase from 114 ± 4 ppbv to 147 ± 6 ppbv. The ice-core multisite CO record exhibits an excellent overlap with

the atmospheric CO record from Greenland firn air which spans the 1950-2010 time period. The combined ice-core and firn air CO history, spanning 1700-2010 CE provides useful constraints for future model studies of atmospheric changes since the preindustrial period.

1   Introduction

Carbon monoxide (CO) is a reactive trace gas that plays a crucial role in the interactions between climate and atmospheric chemistry. CO strongly affects the global oxidative capacity of the atmosphere by acting on the budgets of both hydroxyl radical (OH) and ozone (O_3). CO is the principal sink for the tropospheric OH, with up to 40% of the OH radicals reacting with CO in the modern troposphere (Lelieveld et al., 2016). Thus, CO indirectly impacts the lifetime of numerous atmospheric constituents such as methane (CH4), non-methane hydrocarbons (NMHCs), and hydrofluorocarbons (HCFCs). Oxidation of CO by OH ultimately leads to CO2 production, and in the presence of high levels of nitrogen oxides (NOx) can also result in significant production of tropospheric ozone (Crutzen, 1973). Since CO impacts the atmospheric budgets of greenhouse gases such as CO_2, CH_4 and tropospheric ozone, its present-day emissions lead to an indirect radiative forcing of about 0.23 ± 0.05 W m^{-2} (Myhre et al. 2013). Furthermore, CO has another indirect climatic impact through the formation of submicron secondary organic aerosol produced by oxidation of volatile organic compounds (VOCs).

CO is emitted by various surface processes and produced by atmospheric oxidation of different gaseous precursors. Atmospheric oxidation of CH_4 and VOCs represents about half of the sources (Duncan et al., 2007). The surface sources include incomplete combustion of anthropogenic fossil fuels and biofuels (Hoesly et al., 2018), biomass burning (van der Werf et al., 2017), and minor contributions from plant leaves (Tarr et al., 1995; Bruhn et al., 2013) and the ocean (Conte et al., 2019). The oxidation by OH is the dominant sink of CO, which results in a mean global CO tropospheric lifetime of about 2 months (Khalil et al., 1999). However, the CO lifetime strongly varies with latitude and season, ranging from 20–40 days in the tropics and up to 3 months in polar areas (Duncan et al., 2007).

The understanding of the past CO trends is crucial for monitoring how anthropogenic activities have impacted CO emissions, atmospheric chemistry and composition. Over the last decades, analyses of past CO trends have been made possible by a growing number of direct and indirect observations. Monitoring of atmospheric CO, initiated by NOAA (National Oceanic and Atmospheric Administration) in 1988, revealed a global decrease of tropospheric CO by $\sim$0.5 ppbv yr^{-1} between 1988 and 1996 (Novelli et al., 1998). The space-born MOPITT (Measurements of Pollution in The Troposphere instrument) has monitored the atmospheric CO burden since 2000 (Deeter et al., 2017), and reveals a declining trend. This trend is more pronounced in the Northern Hemisphere (Zheng et al., 2019) which concentrates more sources related to the global economic activity such as fossil fuel use and CO emission from combustion processes.

Ground based and satellite-derived CO data are only available, however, for the last three decades. Ancient air preserved in glacial ice and firn is thus a unique archive for reconstructing the past atmospheric CO record prior to the 1990s. The firn is the upper layer of an ice sheet where snow is slowly transformed into ice. A large amount of air can be sampled from the interconnected open pores. Mean ages of atmospheric gas increase with firn depth. CO has only been measured in firn air at a

few Northern Hemisphere sites, including Summit, the North Greenland Ice Core Project (NGRIP), and the North Greenland Eemian drilling site (NEEM) (Petrenko et al., 2013). Measurements performed on the Devon Island (Canadian Arctic) firn air showed CO artefacts precluding atmospheric reconstruction (Clark et al., 2007). The three central Greenland firn records allowed for a 60 yrs reconstruction of atmospheric CO and revealed that atmospheric CO mixing ratios in the Arctic following industrialization increased from 145 ppbv in 1950 CE (Common Era) until around the late 1970s with a peak of 155 ppbv, and decreased to 140 ppbv in the late 1990s. This decreasing trend in atmospheric CO mixing ratio reconstructed from firn archive is in agreement with direct observations (ground and satellite based) for the last decades. Isotopic measurements of the NEEM firn air suggested this pattern was driven mainly by a change in CO emissions derived from fossil fuel combustion (Wang et al., 2012).

Analysis of air trapped in bubbles in solid ice below the firn layer is required to extend such reconstruction further back in time, beyond 1950 CE. The pioneering measurements conducted on the Eurocore ice archive (Haan et al., 1996; Haan and Raynaud, 1998) found that Northern Hemisphere (NH) [CO] increased gradually from ∼90 ppbv in 1850 CE to 110 ppbv in ∼1950 CE and that CO levels were stable at ∼90 ppbv from 1625 to 1850 CE. Air older than 1600 CE (below 167 m depth) exhibited higher variability and elevated CO levels (100–180 ppbv) with parallel anomalies in the CO_2 record. This section of the Greenland Eurocore record is thought to reflect in situ CO production rather than an atmospheric signal. Haan and colleagues determined CO concentrations along the Eurocore archive using gas chromatography, including a mercuric oxide detector, combined with wet extractions of the trapped gases from discrete pieces of ice. This protocol was affected by a relatively large blank (typically 10 ppbv), was time consuming and resulted in limited resolution reconstructions.

Over the last decade, Continuous Flow Analyses (CFA) of ice core CH_4 concentrations utilising laser spectroscopy (Stowasser et al., 2012) has become a widely-used tool in palaeoclimatology (e.g., Rhodes et al., 2015). CFA was applied for the first time to CO with the measurement from the NEEM-2011-S1 core (Faïn et al., 2014), as an attempt to reconstruct an atmospheric history for NH CO over the past 1800 yrs. The ultra-high resolution of CFA analysis means it is a powerful tool to distinguish between depth sections impacted by in situ CO production and sections preserving the atmospheric record. Faïn et al. (2014) report stable measurements of CO mixing ratios with an external precision of 7.8 ppbv (1σ), but a poorly constrained procedural blank and poor accuracy because absolute calibration was not yet possible. The NEEM-2011-S1 CO mixing ratios reported are highly variable throughout the ice core with high frequency (at the annual scale), high amplitude spikes characterizing the record. These CO signals likely result from in situ production occurring within the ice itself, with patterns too abrupt and rapid to reflect atmospheric variability. In situ production coupled with the procedural blank and accuracy problems largely prevented interpretation of the record in terms of atmospheric CO variations.

In this study, we expand on this exploratory investigation by reporting continuous CO data measured on a set of five additional Greenland ice cores. By combining the analysis of these new ice core records, and separating the high frequency CO signals driven by in situ production from baseline concentrations, we reveal in the Arctic and for the last three centuries (i) an upper bound estimate of past atmospheric CO abundance and (ii) atmospheric [CO] trends. Climate-chemistry models and/or Earth System Models can produce simulated atmospheric [CO] at ground level in Central Greenland, from the preindustrial era to present-day. Such models are presently intercompared within the AerChemMIP exercise (Collins et al., 2017). The compar-

ison of the past evolution of Arctic atmospheric CO mixing ratio extracted from Greenland ice archives in the frame of this study with AerChemMIP model outputs is out of the scope of this paper. Such comparison, which should also allow to better constrain CO emissions inventories of emissions factors, will be addressed in a future study.

2 Methods

2.1 Sample description

Five ice cores extracted from Greenland (Table 1) were investigated in this study (Fig. S1). High resolution CO mixing ratio data were measured continuously along with those of methane. The methane data for the NEEM-SC, D4, North Greenland Ice Core Project (NGRIP), and Tunu13 sites have been reported previously (Rhodes et al., 2016). The NEEM-SC section was chosen to extend the existing NEEM-2011-S1 record (Faïn et al., 2014; Rhodes et al., 2013) further back in time, and a composite NEEM signal including the NEEM-2011-S1 and new NEEM-SC sections is presented here. The calibration of the NEEM-2011-S1 CO data was revisited before building this composite (see Supplementary Information, SI Sect. 2.1). The NEEM-SC and NEEM-2011-S1 archives are different ice cores, but drilled at the same location.

The fifth ice core in this study is a new core, retrieved from central Greenland during June 2015: the PLACE ice core. The PLACE core was drilled 1 km away from the location of Eurocore site(72.58°N and 37.64°W, drilled 1989; Schwander and Rufli, 1994), which in prior work was suggested to contain an intact atmospheric CO signal for air ages younger than 1650 CE (Haan et al., 1996; Haan and Raynaud, 1998). Care was taken when selecting the PLACE site to avoid drilling in areas that were disturbed during the Eurocore and later GRIP ice core drilling operations. The core sections were drilled with the Blue Ice Drill (BID) (Kuhl et al., 2014) and immediately placed in the shade in a clean snow area after drilling, before packing in ice core boxes. These boxes were then stored in a snow cave (at -20°C or colder). At the end of the season, the cores were removed from the snow cave at the field site and returned to Summit Station for transport to the National Ice Core Laboratory (NICL), Denver, CO USA. Core temperature was verified to not have exceeded -15°C during transport by including temperature loggers in some of the ice core boxes.

The five sites investigated experience accumulation rates ranging from 8 to 41 cm weq yr^{-1}, mean annual surface temperature between -24 and -32°C, and different chemical composition (Table 1, Sect. 3.3). Description of the ice and gas chronologies for the five ice cores is reported in Table S1.

2.2 CO continuous flow analyses

Since the first continuous, high resolution, CO measurements were performed along the NEEM-S1 ice core in 2011 (Faïn et al., 2014), CFA-based CO analyses have greatly improved, including lowering the CO blank and characterizing how CO is preferentially dissolved during the CFA process so as to establish an absolute calibration. The excellent precision of CO analyses has been confirmed, and the designs of CFA setups themselves have been optimized to limit the instrumental smoothing and

Table 1. Locations, site characteristics and other relevant information for ice cores featured in this study.

Ice core and location	Drilling year	Depth interval (m)	Gas age interval (yrs CE)	Accum. rate (cm ice yr^{-1})	Mean annual Temp. (°C)
D4 Central Greenland 71.40°N, 43.08°W 2713 m elevation	2001	63-145	1825;1961	41[a]	-24[a]
Tunu13 NE Greenland 78.03°N, 33.88°W 2200 m elevation	2013	61-213	836 ; 1893	8-14	-29[b]
NGRIP Central Greenland 75.10°N, 42.32°W 2917 m elevation	2000	74-108 207-254 519-569 1215-1265	1780 ; 1926 980 ; 1237 -929 ; -616 -5545 ; -5899	19[c]	-31.5[c]
PLACE Central Greenland 72.58°N, 37.64°W 3200 m elevation	2015	80-153	1447;1957	20.5	-32
NEEM-2011-S1 NW Greenland 77.45°N, 51.06°W 2450 m elevation	2011	71-409	270 ; 1961	22[d]	-28.9[d]
NEEM-2011-SC NW Greenland 77.45°N, 51.06°W 2450 m elevation	2009	399-573	-682 ; 322	22[d]	-28.9[d]

[a] Rhodes et al. (2016); [b] Butler et al. (1999); [c] community members (2004); [d] NEEM community members (2012).

improve signal resolution. This section reviews the operation and recent improvements of CFA-based CO measurements. More details can also be found in Supplementary Information (SI Sect. 1).

2.2.1 System operation

The ice cores listed in Table 1 were analysed using continuous ice core melter systems coupled with online gas measurements. The general principles of this analytical approach are provided by (Stowasser et al., 2012). Briefly, ice core sticks are cut at a 34 mm x 34 mm cross section and processed on a melterhead located in a cold room. The melterhead is composed of inner and outer collection areas with the inner area dedicated to sample collection. To prevent contamination, an overflow from the inner to the outer melterhead areas of >10% is created by lowering the sample pumping speed. The water and gas bubble mixture is continuously pumped via a debubbler into a temperature-controlled gas extraction unit maintained at 30°C. The gas/water volume ratio of the sample is about 10% before the debubbler, and 50% after the debubbler. A fully degassed fraction of the melted sample is thus also available at the debubbler for complementary chemical analyses in the liquid phase. The gas is recovered from the sample line after the debubbler by applying a pressure gradient across a gas-permeable membrane, either Transfer-Line (Idex) or Micromodule 0.5×1 (Membrana GmbH) degassers. Then, the gas is dried by a custom-made Nafion (Perma Pure) dryer. Finally, CO (and/or CH_4) mixing ratios are continuously monitored along the gas sample flow by a laser spectrometer.

Our samples were all analysed at the Desert Research Institute (DRI), Reno (NV, USA) during two analytical campaigns (Tunu13, D4, NEEM-SC, and NGRIP in 2013; PLACE in 2015). The NEEM-2011-S1 core was analysed at DRI in 2011, as described by Faïn et al. (2014). The PLACE core was also analysed at the Institute of Environmental Geosciences (IGE, Grenoble, France) in 2017. Specific descriptions of the DRI and IGE setups were already provided by Rhodes et al. (2015) and Fourteau et al. (2017), respectively, and a comparison of the two setups is reported in the SI Sect. 1.2.

A unique spectrometer, using optical feedback cavity enhanced absorption spectrometry (SARA, developed at Laboratoire Interdisciplinaire de Physique, University Grenoble Alpes, France; Morville et al., 2005) was used to analyse carbon monoxide (and simultaneously, methane) at both DRI and IGE and during the three analytical campaigns. Detailed description of this instrument, which was used for CO measurements along the NEEM-2011-S1 core in 2011 at DRI, is reported by Faïn et al. (2014). The OF-CEAS instrument was always carefully calibrated against standard gases (Table S3) before melting ice cores (see SI Sect. 1.4).

2.2.2 Calibration Loop

The degassing membranes operated so far in gas-CFA systems extract bubbles from the sample flow but do not recover dissolved gases from the water phase efficiently. Carbon monoxide (or methane) have higher solubility than N_2 or O_2. Consequently, mixing ratios of CO in the gas phase of the sample flow exhibit lower values than initially existing in the ice bubbles. These offsets need to be corrected for, and an attempt to replicate the conditions experienced by the ice core water-gas mixture between the melterhead and the laser spectrometer was reported originally by Stowasser et al. (2012). As melting ice contains 10% air by volume, a 10:90 mixture of synthetic air and degassed deionized (DI) water can be introduced into the system via a 4-port valve located directly after the melterhead. The water is sourced from a 2 L reservoir degassed by constantly bubbling ultra-pure He through it. The air–water mixture follows the same path through the system as the ice core sample before being

analysed by the laser spectrometer. However, it is not completely identical as it includes more components such as an additional peristaltic pump or extra lines. This pathway for synthetic standard analysis will be referred to as "calibration loop" here, but has been designated as "full loop" in previous studies (e.g., Rhodes et al., 2013; Faïn et al., 2014). Note that this "calibration loop" should not be confused with the "Internal Loop" (Rhodes et al., 2013) a system to isolate the gas extraction system from the remainder of the melting system, while keeping a continuous gas extraction (see Fig. 1 from Rhodes et al., 2013).

2.2.3 CO blank of CFA-based analyses

The CO procedural blank was evaluated for each analytical campaign. Two different evaluation approaches were applied, which are described in SI Sect. 1.5. A relatively high CO blank of 35±7 ppbv was observed at DRI in 2013, when using a Membrana Micromodule degasser for analysing the Tunu13, D4, and a fraction of the NEEM-SC cores. Lower blank values, ranging 4.1±1.2 to 12.6±4.4 ppbv were observed when using an Idex Transfer-Line degasser (cores PLACE, NGRIP, a fraction of NEEM-SC).

2.2.4 Internal precision and stability

Internal precision and stability of gas-CFA measurements can be evaluated by Allan variance tests (Allan, 1966) applied to the calibration loop dataset. Laser spectrometers produce many measurements per minute, with a data acquisition rate of 6 Hz for our OF-CEAS instrument. Observed optimal integration time (i.e., time of lowest Allan deviation) was determined for each analytical campaign, and is now larger than 500 s for DRI, and 1000 s for IGE CFA setups (SI), which is much longer than the 5 s reported by Faïn et al. (2014) and testament to increased stability. However, to maximize the depth resolution, CO data can be averaged over shorter integration time (IT). There is a trade-off between internal precision and IT. Abrupt, non-climatic signals in gas records, such as in situ CO production (Faïn et al., 2014), cannot be fully resolved without reducing the IT. Internal precision, defined as twice the Allan deviation at chosen integration times, ranged from 1.2 to 1.6 ppbv depending on the analytical campaign (SI Sect. 1.6 and Table S2).

2.2.5 External precision

External precision of the continuous CO measurements (i.e., including all sources of errors or bias) was investigated by melting replicate ice sticks on different days during each analytical campaign. Specifically, we defined the external precision as the pooled standard deviation calculated on the differences of CO concentrations from main and replicate analysed ice sticks, averaging continuous CO data over few cm long intervals (SI Sect. 1.7). This approach estimates an external precision of 5.7 ppbv for the DRI gas-CFA setup in 2011 (NEEM-2011-S1 campaign, 18 m long replicated section, using 9 cm intervals). We reproduced this analysis for the 2015 DRI campaign, and established an external precision of 6.6 ppbv (19.6 m long replicated section, 10-cm long intervals, Fig. S3). With a similar methodology, but a shorter replicate section analysed, we evaluated the external precision of PLACE continuous CO measurements conducted at IGE in 2017 to 3.3 ppbv (2.3 m long replicated section, 1-cm intervals, Fig. S3). No replicate ice core sections were available and measured during the 2013 DRI campaign.

For the 2013 campaign, we consider the external precision to be 5.7 ppbv for the ice cores analyzed in 2013 with a Micromodule and 6.6 ppbv using the Idex Transfer-Line degasser, by extrapolating results from similar CFA setups.

2.2.6 Absolute calibration and accuracy

CFA–based gas records must be corrected for under-recovery of gases dissolved in the water stream to obtain absolute values on the WMO-CO X2014A calibration scale. The magnitude of gas dissolution is monitored using the calibration loop (Sect. 2.2.2). In this study, a 73 m long ice core (PLACE) was analysed on two different CFA setups (at IGE and DRI), for CO but also for CH_4 mixing ratios. This gas CFA laboratory intercomparison revealed that the fraction of CH_4 not recovered at IGE was larger than at DRI (14% and 10%, respectively). Note that the gas extraction unit and OF-CEAS detection instrument were identical, and only the melter and lines upstream of the Idex Transfer-line degasser had different geometries (Sect. 2.2.3). This intercomparison demonstrates that the solubility-based calibrations are required to transfer gas CFA datasets into absolute concentration scales, and are dependent on the geometry and operation of a CFA setup. This observation was further confirmed at IGE by measuring the CH_4 mixing ratio at IGE when melting replicate ice sticks with varying CFA system geometries (eg., length of lines) and operation of the CFA setup (e.g., melting speed, pumping rate). For each analytical campaign, the geometry and operational protocol of the CFA setup were thus kept unchanged during the measurements. However, these observations rule out universal modelling of the preferential CO dissolution by using Henry's Law coefficient, and demonstrate that CFA setups are dynamic systems, not at solubility equilibrium.

In this study, we used the calibration loop operated with standard gases (Table S3) for absolute calibration of the CO dataset. Such an approach has been successfully applied for CH_4 (e.g., Rhodes et al., 2015). However, calibration loops need to be carefully set up and operated, to closely reproduce solubility losses occurring in the CFA sample pathway. In the case of CH_4, discrete datasets often allow for an external validation of this CFA internal calibration, but such validation was not available for Greenland CO. We hypothesise that CO and CH_4 dissolution follow the same physical laws: consequently, if a calibration loop is able to reproduce methane preferential dissolution, it should also reproduce CO losses related to dissolution. Thus, calibration loop experiments reproducing the expected methane preferential dissolution were conducted for each analytical campaign. We extracted from such calibration loop experiments solubility calibration (SC) factors for CO. Overall, CO losses driven by preferential dissolution ranged from 4 to 9%. Replicate measurements show that the fraction of CO not recovered at the outlet of the CFA system was very stable during analytical campaigns, both at DRI and IGE. Based on repeated calibration loop measurements throughout the campaigns we conservatively estimate the uncertainty of the SC factor to be $\pm1\%$ (2 sigma). To further evaluate the robustness of the CFA procedure and this absolute calibration approach, five discrete samples of the PLACE core were analysed with a discrete CO setup (SI Sect. 1.8.4, Fig. S7). The agreement between discrete and CFA-based CO dataset (both IGE and DRI) was excellent, with differences in CO mixing ratio ranging from 0.4 to 2.8%. The depth intervals of the discrete samples encompassed the entire span of the PLACE core, from 84 to 146 m depth. More details about absolute CO calibration are reported in Supplementary Information (SI Sect. 1.8).

2.2.7 Signal Smoothing

The mixing of gases and meltwater during the sample transfer from the melt head to the laser spectrometer induces a CFA experimental smoothing of the signal. The extent of the CFA-based damping was determined for each analytical campaign by performing step tests, i.e., switches between two synthetic mixtures of degassed DI water and synthetic air standards of different CH_4 concentrations (Stowasser et al., 2012, see SI Sect. 1.9). A cut-off wavelength can be defined as the wavelength of a sine signal experiencing a 50% attenuation in amplitude. Cut-off wavelengths ranged from 15.0 cm during the DRI 2013 campaign (when using Membrana Micromodule degasser) to 1.6 cm during IGE 2017 campaign (Table S2). Lower cut-off wavelengths were obtained by limiting system dead volume, most notably by reducing the debubbler internal volume and by using an optimized Idex Transfer-Line degasser instead of Membrana Micromodule degasser (1 and 5 ml internal volume, respectively)

2.2.8 Data processing

CO and ice chemistry data collected at DRI were mapped onto depth scales using high-resolution (0.1–0.5 Hz acquisition rate) liquid conductivity data and time–depth relationships recorded by system operators. A constant melt rate for each metre length of core is assumed. DRI depth scale uncertainties are estimated to be ± 1 cm (1σ).

Occasional entry of ambient air into the analytical system as breaks in the core were encountered caused contamination. The OF-CEAS spectrometer simultaneously measures CO and CH_4 mixing ratios, and such contamination was characterised by a sharp increase in CH_4 concentration (ca. 1900 ppbv) followed by an exponential decrease. Data were manually screened for these ambient air contamination events.

Uncertainty on CO mixing ratios is established as 1σ and calculated for each calibrated CO dataset. It combined uncertainties evaluated specifically for each analytical setup on CO blanks, solubility calibration factors, and internal precision of CO CFA measurements (see SI and previous sections).

Finally, we used high resolution water isotope datasets to match DRI and IGE PLACE depth scales. Water isotopic ratios were measured simultaneously with gas concentrations in both laboratories using laser spectroscopy (Gkinis et al., 2011; Maselli et al., 2013).

2.3 Investigation of possible rapid CO production from trace organics in the ice during melting

To investigate if elevated or highly variable carbon monoxide levels observed in Greenland ice core could originate from the melting process (i.e., "in extractu" CO production from trace organics in the ice), CO concentrations were determined in tests with 20 discrete ice and firn samples (sized between 272 - 1089 g, average size of 690 g). The experimental protocol is reported in detail in the SI. Briefly, ice samples collected below close-off depth (fully closed porosity) are completely grated to fine powder to remove trapped air. Firn samples do not contain a significant amount of trapped air; however some firn samples were still grated to powder to verify that the grating process did not increase the [CO] blank. The samples are then introduced in a glass vessel, evacuated and flushed with ultrapure air overnight. Gas standard of known concentration is then introduced

within the vessel. Consequently, for both firn and ice samples CO mixing ratio within the vessel prior to melting is equal to that of the gas standard introduced in the vessel. If CO in extractu production occurs during melting, it should cause an increase in
250 CO mixing ratio above this known value.

The CO concentration in the gas available in the vessel headspace is determined by gas chromatography combined with a mercuric oxide reduction detector (RGD; Peak Performer 1 from Peak Laboratories), at three different stages: before melting, during melting, and after melting. CO concentrations are calibrated using four synthetic air gas standards with nominal CO concentrations ranging from 50 to 500 ppbv, and data are reported on the WMO-CO X2014A scale.

255 Three large diameter (27 cm) cores collected with the Blue Ice Drill (BID) were used for these tests: the PLACE ice core (Central Greenland, Table 1), the C14 firn core (Central Greenland, drilled in June 2015, 72°39.62' N, 38°34.85' W), and a Taylor Glacier ice core (Antarctica, drilled in December 2015, 77˚45.69' S, 161˚43.18' E). BID cores allowed for up to four true depth replicates to be measured from the same depth interval. CO concentrations were determined (before, during, and after melting) for the following cases: (i) Greenland C14 firn (45 m depth), (ii) Greenland PLACE ice from depths ranging
260 110-125 m and showing low and stable [CO] on the continuous CFA record, (iii) Greenland PLACE ice from depths (111 m) showing elevated and highly variable [CO] on the continuous CFA, (iv) Oldest Dryas (15 kyrs BP) and Holocene (9.5 kyrs) Antarctica ice, and (v) gas-free ice made from degassed Milli-Q 18.2MΩ.

2.4 Chemistry data

During the two DRI analytical campaigns, melted ice core samples were analysed continuously by inductively coupled plasma
265 mass spectrometry (ICP-MS) and CFA for chemical species. These analytical methods have been reported previously (Mc-Connell and Edwards, 2008; McConnell et al., 2007, 2002). High-resolution measurements of total organic carbon (TOC) were obtained at DRI by coupling a Sievers 900 TOC analyzer to the DRI ice core melter (Legrand et al., 2016).

3 Results and Discussion

The new CO records available from the PLACE, NGRIP, NEEM, D4, and Tunu13 ice-cores are reported in Fig. 1 and plotted
270 for the period spanning 1650 to 1960 CE (gas age, see Table S1). Only the NEEM, NGRIP and Tunu13 datasets significantly extend beyond the last three centuries and the full records are reported in Fig. S17. Over the 1650-1960 CE period, all Greenland CO ice records exhibit highly variable CO values. A minimum mixing ratio of 92 ppbv is observed at NEEM and PLACE, and a maximum mixing ratio of 1191 ppbv at Tunu13. Considering all records, some 46 events revealed mixing ratios higher than 250 ppbv. In Sect. 3.1 we discuss the baseline CO levels of the different ice-core records, and the characteristics of abrupt
275 CO spikes detected in all records. Tests and discussions presented in Sect 3.2. demonstrate that in situ production drives these abrupt CO spikes. The key question of whether an atmospheric signal can be extracted from the low frequency variability of the CO ice-records' baselines is discussed in Sect. 3.3. Comparison of our new CO records with existing data is presented in Sect. 3.4. Finally, a multi-site reconstruction of past atmospheric CO levels at northern latitudes is presented in Sect. 3.5.
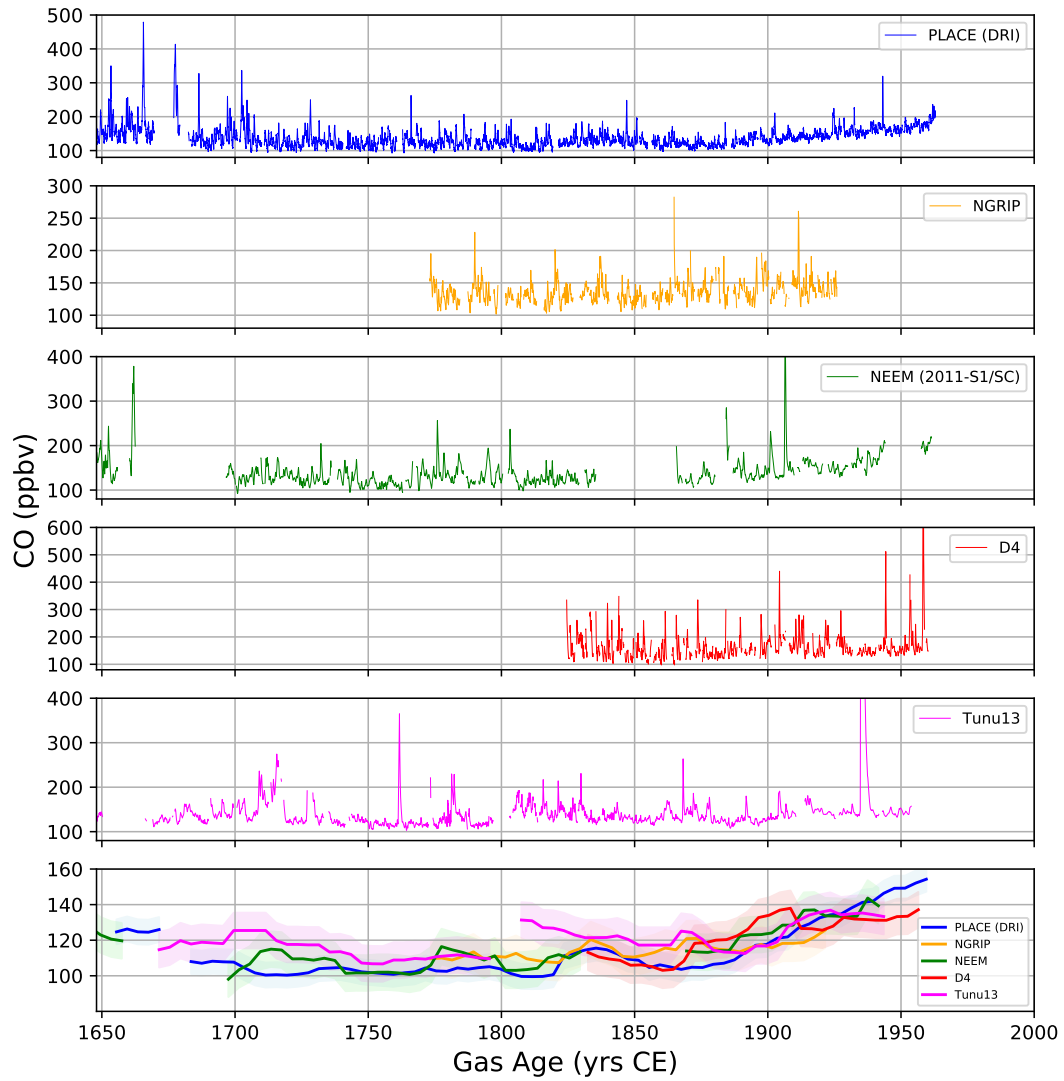
Figure 1. Upper panels: Greenland continous CO records available from the PLACE (DRI), NGRIP, NEEM, D4, and Tunu13 ice-cores and plotted for the period spanning 1650-1960 CE. Lower panel : CO baseline levels from each ice-record defined as the 5th percentile of data every 4 years over a moving window of 15 yrs, with shaded envelopes reported on each baseline representing the uncertainty.

3.1 Continuous CO records along Greenlandic ice cores

 #### 3.1.1 CO baseline levels

We identified the CO baseline levels from each ice-record by calculating the 5th percentile of data every 4 years over a moving window of 15 yrs. A window of 15 yrs corresponds to a time interval shorter than the full width at half maximum of the CO age distribution at these sites (Table 1). We chose to use 5th percentile CO baselines because they can be calculated identically for all datasets and are not based on the subjective operator decisions involved in identifying and removing peaks to derive a baseline level. The temporal trends in records calculated using 10th percentiles are similar. 5th percentiles were not computed when more than 50% of the data were missing within the windows. Figure 1 (lower panel) reports 5th percentile CO baselines extracted over the last 300 years from the D4, Tunu13, NGRIP, NEEM, and PLACE ice-records (all DRI dataset). The shaded envelope reported on each baseline represents the uncertainty (1σ) calculated by propagating CO external precision and uncertainties on CO blank and solubility calibration factor (see Sect. 2). The CO baseline records from the five ice cores are always within 20 ppbv of each other. From 1700 to 1875 CE, the ice-records indicate rather unchanged or slightly enhanced levels with time, whereas from 1875 to 1950 CE, all the ice-records reveal a steady increase.

3.1.2 High frequency non atmospheric CO signals

Figure 1 shows that the five Greenlandic sites investigated in this study all exhibit highly variable CO mixing ratios. Referring to previous data reported by Faïn et al. (2014), such a pattern was expected when measuring the NEEM-SC samples and extending the NEEM-2011-S1 record. However, new records from central Greenland (PLACE, NGRIP), north-eastern Greenland (Tunu13) and southern Greenland (D4) appear to be also affected by variability in CO mixing ratios that is too large and rapid to reflect past atmospheric mixing ratio changes (Figs. 1 and S17).

The true extent of high CO variability may be masked, however, by CFA analytical smoothing. Figure 2 (upper panel) reports a 1.5 m long section of the PLACE ice-core, analysed with both DRI and IGE CFA setups. The higher CFA setup resolution at IGE (Sect. 2.2.7) reveals more features, but may still miss even higher frequency variability and dampen extrema values. Similarly, a CO record from a core drilled at a relatively low snow accumulation site will appear more smoothed out by CFA analysis than one from a relatively high snow accumulation rate site.

High frequency variability within CO records can be quantitatively characterized using MAD (Median Absolute Deviation). MAD calculated for all CO records collected at DRI every 4 yrs over a moving window of 15 yrs (similarly to baseline signals, see Sect. 3.1.1) are reported on Fig. S18. We observe for the 1700-1950 CE time period that NEEM, NGRIP, Tunu13 and PLACE records exhibit stable and similar MAD values, with mean MAD values over the entire 1700-1950 CE period ranging 9.9-14.2 ppbv, depending on the records. The D4 MAD values are larger, varying from 10 to 30 ppbv. The NEEM, NGRIP and Tunu13 datasets significantly extend beyond the last three centuries and reveal different MAD patterns for age older than 1700 CE. The Tunu13 record, spanning the last 1300 yrs, reveals that CO variability remains stable as depth increases while NEEM and NGRIP show increasing MAD with depth, clearly indicating that high variability in CO is more pronounced for
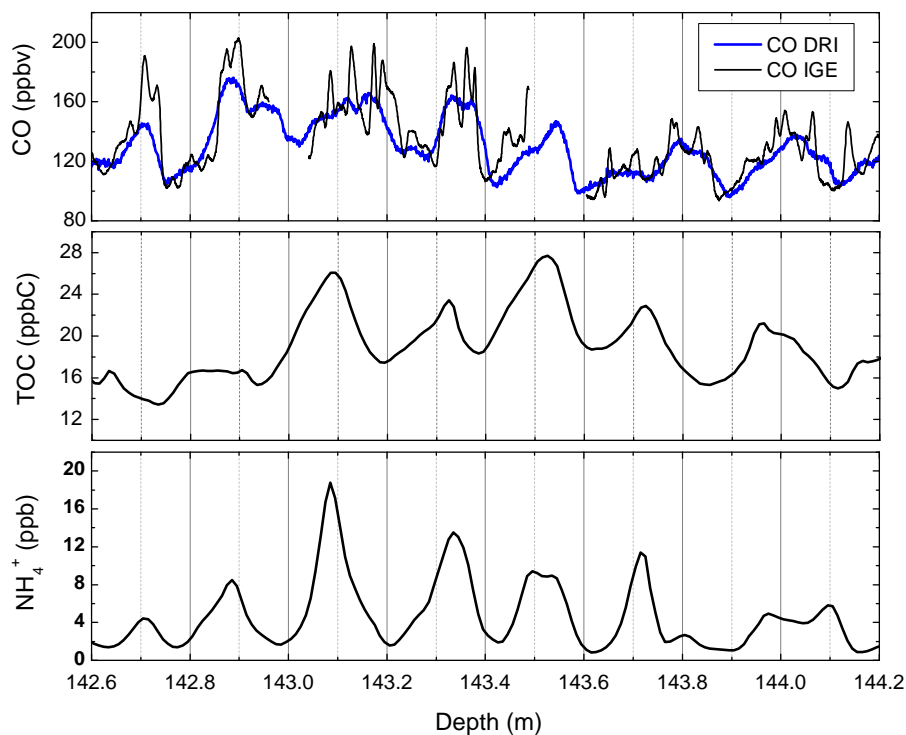
Figure 2. High-resolution TOC, NH_4^+, CO from the PLACE core. CO mixing ratios were measured with both the DRI and IGE CFA systems. NH_4^+ shows a well-marked seasonal cycle characterized by a summer maximum. PLACE snow accumulation is about $20\,\mathrm{cm\,weq\,yr^{-1}}$

.

older ice. These increases are significant, with MAD values reaching ~ 60 ppbv for the deeper sections of the analyzed NEEM and NGRIP ice-core sections.

3.2 Do drilling or analytical processes cause CO production?

The observation of high frequency CO variability along the NEEM-2011-S1 core led Faïn et al. (2014) to discuss if such patterns could be driven by the processes involved in sample collection and analysis. Here we consider our new data to assess in more detail if such processes can drive CO production.

3.2.1 Ice core drilling

We observe that abrupt CO spikes of similar magnitude occur in ice-cores extracted by dry drillings (e.g., PLACE, D4, Tunu13) and when a drilling fluid was used (e.g., NEEM, NGRIP) (Fig. 1). This clearly rules out contamination from the drilling fluid as a cause for high frequency CO variability, confirming the previous conclusion from Faïn et al. (2014).

Haan et al. (2001) observed CO production within an alpine snowpack in daylight. Drillings are usually conducted at high-altitude sites in summer where UV radiation levels are high. One could thus hypothesise that CO is photochemically produced

within ice-cores just after drilling, when ice-cores are handled at the drilling site before being packed in ice-core boxes. During the PLACE and NEEM-SC drillings, ==specific care was taken to never expose freshly drilled cores to direct sunlight.== For PLACE, a shaded area was set up for core processing. NEEM 2011-S1 and SC core drillings were conducted in a tent and a trench, respectively. In spite of that, all these ice-cores reveal CO spikes. In contrast, no specific care was taken during the historical Eurocore drilling when handling cores, with respect to sunlight exposure, and Haan and Raynaud (1998) report that this archive does not exhibit highly variable CO concentration in the upper section. Based on this, it appears that brief direct exposure to sunlight after drilling is unlikely to be the cause of the large CO spikes

3.2.2 Impact of long-term core storage

By comparing the storage time of different ice-cores (storage without light exposure) prior to CO analysis with the same CFA setup (NEEM-2011-S1 and D4), Faïn et al. (2014) concluded that CO production in ice during core storage was unlikely. We extend this observation by comparing central Greenland archives: NGRIP and PLACE records reveal similar abrupt CO spikes and CO baselines (Fig. 1) while PLACE and NGRIP cores were analysed 3 months and 15 years, respectively, after drilling. Furthermore, we measured at IGE a 10 m long replicate section of the PLACE core nearly two years after the main analytical campaign (respectively December 2018 and February 2017) and no change in the CO values was observed (Fig. S14).

3.2.3 Impact of CFA process

In 2013 at DRI, a 4 m long replicate section of the D4 ice-core was melted with all laboratories kept in darkness. Similar in situ CO production patterns were observed under light and dark melting conditions. These results, already reported by Faïn et al. (2014, Fig. S2), reveal that CO variability observed along the D4 core are not related to photochemically driven CO production occurring in the sampling lines between the melter head and the CFA extraction box. To further evaluate if the CFA analytical system could somehow induce CO production within the melted ice, a melted D4 sample was collected downstream of the degassing membrane and re-circulated in the calibration loop mode (Sect. 2.2.2) for one hour as degassed blank water. We observed similar CO levels to the deionised water blank.

3.2.4 Results of investigation of possible rapid CO production from trace organics in the ice during melting

As described above, CO analyses of 20 discrete ice and firn core samples (including the PLACE core) were carried out at the University of Rochester, with the goals of investigating the possibility of in extractu production of CO from trace organics in the ice during melting of ice core samples (Sect. 2.3 and SI Sect. 1.11, Table S4).

All of the different ice and firn sample types, including samples of different mass and a gas-free ice sample, showed a consistent excess CO growth occurring during the melting step, with excess CO increasing by 6.4 ppbv on average (Fig. 3) - a much smaller CO enhancement than the spikes observed in the CFA records. Since the excess CO produced appears stable after melting, and consistent between the sample types, the excess CO observed is likely a systematic extraction system blank. If the CO production mechanism involves organic compounds present in the ice lattice, it would be expected that variations in
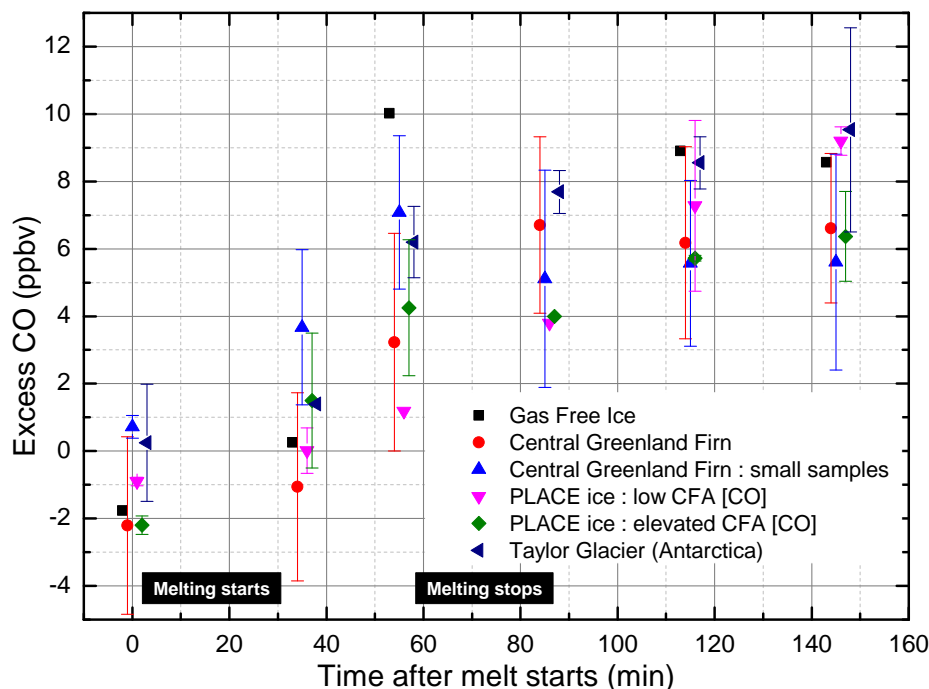
Figure 3. Average excess in CO mixing ratios produced during melting of discrete samples measured by gas chromatography combined with a mercuric oxide reduction detector. The CO values shown have been corrected for a small (~ 3 ppbv) CO excess observed in equivalent tests where the ice samples were not melted (see SI Sect. 1.11.3). The following samples are investigated : gas free ice, firn from Central Greenland (including low mass samples), PLACE ice samples exhibiting high CFA [CO] and low CFA [CO], Taylor Glacier (Antarctica) ice. Samples description is reported in Table S4. Error bars represent one standard deviation for all sample runs of a given type and points without error bars represent single measurements

.

the concentrations of organics from samples collected at different sites / from different depth levels, as well as differences in
355   the melted ice mass would result in significant differences in excess CO. Some of the PLACE ice samples were specifically selected for having exhibited low and stable [CO] on the continuous CFA record while others were selected for exhibiting elevated and spiky [CO] behavior suggesting the possibility for instantaneous CO production during melting (Fig. 3, Table S4). The other samples, the two Taylor Glacier and gas-free ice were also selected as they should have very different trace organic loadings to the Greenland ice, especially the gas-free ice sample which have no significant organic loading (< 2 ppbC). Further,
360   replicate firn samples of different mass would be expected to have a total organic loading that scales with the firn mass. Because there are no significant differences observed in the excess CO produced from these very different sample types (Fig. 3), these

results indicate that the melt-extraction process itself does not result in significant CO production from trace organics found within the ice samples. Instead, these results lend further support to the idea that the elevated and highly variable [CO] values observed in Greenland ice samples are due to excess CO produced from in situ production within the ice itself (Faïn et al., 2014; Haan and Raynaud, 1998).

3.3 Atmospheric CO history retrieved from Greenland ice cores

We now explore if past atmospheric concentrations of CO can be extracted from the low frequency variability of the CO ice-records' baselines (Fig. 1). The key question is: does the in situ production present in all five cores still impact the 5th percentile of data that we adopt as a baseline?

In our earlier study on the NEEM-S1-2011 core (Fain et al., 2014), we reported that 68% of the CO spikes were observed in ice layers enriched with pyrogenic aerosols (i.e., exhibiting ammonium levels above 18 ppb). Within the 60 cm length core analysed in that study, elevated ammonium (NH_4^+) and CO were found together with dissolved organic carbon (DOC) (>100 ppbC) representing an important reservoir of carbon, which could potentially be oxidized into CO. The oxidation processes involved, however, remain unidentified. Here we focus on the two cores for which we have obtained reliable total organic carbon (TOC) data (Sect. 2.4). These are interesting cores to compare because they have very different snow accumulation rates: Tunu13 has the lowest accumulation rate, which also varies over time between 8 to 13 $\mathrm{cm\,weq\,yr^{-1}}$, while PLACE is more typical of a Late Holocene Greenland core with a stable accumulation rate of $\sim$20 $\mathrm{cm\,weq\,yr^{-1}}$.

3.3.1 The importance of data resolution

Typical CO, TOC, and NH_4^+ patterns observed along the PLACE core are reported along a 1.6 m section on Fig. 2. Maximum and minimum levels of the three species occur at similar depths. NH_4^+ is commonly used in Greenland ice to identify summer layers that are characterized by a well-marked summer maximum (Legrand and Mayewski, 1997). Investigating summertime and wintertime distributions of [CO] and [TOC] over the full PLACE record confirms that both species share coherent seasonality (Fig. S22 and S26): CO and TOC show lower levels in winter-deposited ice layers, suggesting that at the PLACE site the CO signal preserved in winter layers is more suitable for paleo-atmospheric reconstructions.

Typical CO, TOC, and NH_4^+ variations along the Tunu13 core appear different to those at PLACE (Fig. 4). The seasonal cycle in NH_4^+ is still detectable but the TOC and CO records show much less co-variation than at PLACE. PLACE and Tunu13 TOC were analyzed with the same setup (i.e impacted by the same analytical smoothing), but the lower accumulation rate of Tunu13 results in a larger smoothing of the TOC signal. The higher degree of smoothing in CO relative to PLACE results in part from Tunu13 being analysed with the 2013 DRI CFA setup (Micromodule degasser), which shows a larger response time in the gas phase (Table S2). Similarly to TOC, the effect is compounded by the much lower snow accumulation rate of Tunu13 relative to PLACE - the section of core in Fig. 4 has only 8 $\mathrm{cm\,weq\,yr^{-1}}$. Step tests (Sect. 2.2.7) suggest that for CO a 60% attenuation would be expected for a sine signal of 10 cm wavelength, a depth interval representing >1 yr in this case. The impact of analytical smoothing on Tunu13 CO patterns was further investigated by convoluting a Tunu13-like synthetic CO signal with the Green function of the 2013 DRI CFA setup (Fig. S8, middle panel; Fig. S12). A 5th percentile baseline was

395 extracted from the smoothed synthetic signal produced by this convolution. The baseline obtained is found up to 8 ppbv above the original synthetic signal for depth intervals spanning few meters (Fig. S13), confirming that CFA analytical smoothing can positively bias the Tunu13 baseline CO level. More details about this conceptual experiment are available in Sect. SI 1.9.2.
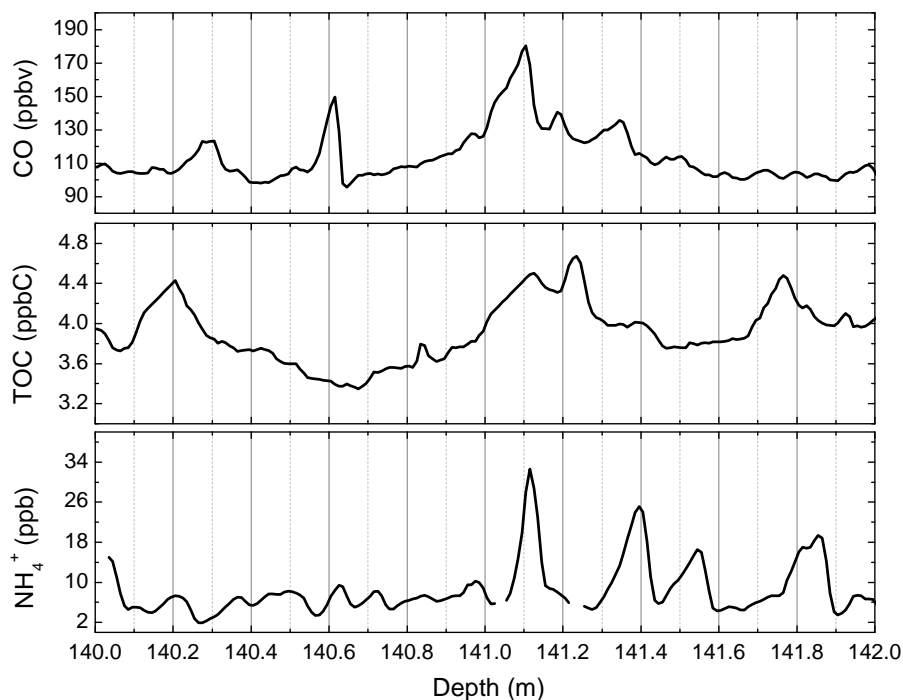
Figure 4. High-resolution TOC, NH_4^+, CO from the Tunu13 core. Snow accumulation is about $8\ \mathrm{cm\ weq\ yr^{-1}}$ at this depth.

The significant analytical smoothing for the Tunu13 ice-core suggests that annual winter minima in CO (associated with winter minima in TOC) may be unresolvable, which would lead to an overestimation of the baseline even when using the 5th per-
400 centile values. In contrast, repeated analyses of the higher snow accumulation PLACE core on two different gas CFA setups (DRI and IGE, Table S2) show that despite the DRI setup (2015 configuration) exerting a greater smoothing effect than the IGE one (SI Sect. 1.9, Fig. S10 and S11), the CO minima values are well-resolved in both cases (Fig. 2). Furthermore, the PLACE CO baseline extracted from the IGE continuous record is similar to the one based on the DRI dataset (SI section 2.4), suggesting that analytical smoothing is not a limitation on isolating CO levels in the winter ice layers at this site. Convoluting
405 a PLACE-like synthetic CO signal with either DRI 2015 and IGE 2017 CFA setup Green function (e.g., SI Sect. 1.9.2) con-
firms this result. This suggests that the 5th percentile baseline calculated at PLACE and other high snow accumulation sites is suitable for investigating past evolutions of the atmospheric CO burden.

3.3.2 TOC patterns and in situ CO production

The high resolution TOC measurements collected along the PLACE core exhibit a stable TOC background value of 13.5 ppbC (baseline defined as the 5th percentile), with 17 spikes above 40 ppbC (70 m long record, Fig. S24). TOC levels observed at Tunu13 are lower, with a baseline value of 7.9 ppbC (1σ) and only 10 spikes above 40 ppbC for a longer record (143 m long record, Fig. S25). Tunu13 mean TOC (10 meters window averaging) exhibits a low frequency variability with values ranging from 4 to 12 ppbC (Fig. 5). The low frequency variability in Tunu13 mean TOC is correlated to changes in the snow accumulation rate (Fig. 5) which varies from 8 to 13 $\mathrm{cm\,weq\,yr^{-1}}$ (annual average). Along most of the core, this linear relationship between TOC and snow accumulation rate remains unchanged, although it becomes steeper below 160 m depth (Fig. S27. Such correlation is not observed at PLACE where the snow accumulation is constant, with annual mean values ranging 20-21.5 $\mathrm{cm\,weq\,yr^{-1}}$.

In situ CO production within Greenland ice archives is very often co-located in ice layers where TOC levels are high (e.g., Fig. 2, S22, and S26) as observed previously on the NEEM-2011-S1 core (Faïn et al., 2014), suggesting that in situ CO production may be related to the organic carbon (OC) availability. The importance of organic carbon in the processes driving CO in situ production is further supported by the long-term averaged mean CO record (running windows of 10 m) which is significantly correlated to mean TOC at Tunu13 (r^2 = 0.56, p<0.01, Fig. 5) for preindustrial times (gas age prior to 1850 CE, i.e. below 83 m depth), with increases in mean CO when TOC and snow accumulation are higher. However, comparison of the Tunu13 and PLACE datasets suggest that higher TOC levels does not always imply higher CO concentrations: over the 1640-1950 CE gas age time period, the mean CO mixing ratio is almost identical for Tunu13 and PLACE (137 and 136 ppbv, respectively) while mean TOC is higher for PLACE compared to Tunu13 (20 and 7 ppbC, respectively). This may suggest that the required amount of OC to lead to significant in situ CO production is already reached at the Tunu13 site.

Characterizing the fate of TOC in Greenland ice is a first requirement for a better understanding of in situ CO production processes. Figure 5 suggests that the fate of TOC deposited at Tunu13 is related to the rate of snow accumulation at the surface. Comparing Tunu13 and PLACE TOC records suggests that the lower the accumulation rate, the lower the TOC baseline concentrations in the deep ice. A snowpit study of recent snow layers deposited at Summit (Hagler et al., 2007) showed that a large fraction of water soluble and insoluble organic carbon may be lost at the surface during post-deposition processes, such as photochemical reactions. We hypothesize that such processes may be enhanced at lower accumulation rates when the snow layers get exposed to UV radiation for longer.

However, the relationships between TOC and ammonium suggest that other processes can impact TOC after deposition at Tunu13. Forest fire debris reaching Central Greenland snow during spring or summer mainly consists of ammonium formate, and organic carbon is mostly made of formate at Summit (Legrand et al., 2016). Legrand and De Angelis (1996) reported a formate-to-ammonium molar ratio close to unity in elevated ammonium events recorded at Summit both during the last 200 years and the Holocene. The relationship between TOC and ammonium at PLACE (Fig. S28) exhibits a similar slope close to unity. A completely different pattern is observed at Tunu13 (Fig. S29), with unexpectedly low TOC observed along ammonium peaks. We suggest that ammonium formate has been remobilized after deposition in the snow at sites with snow accumulation
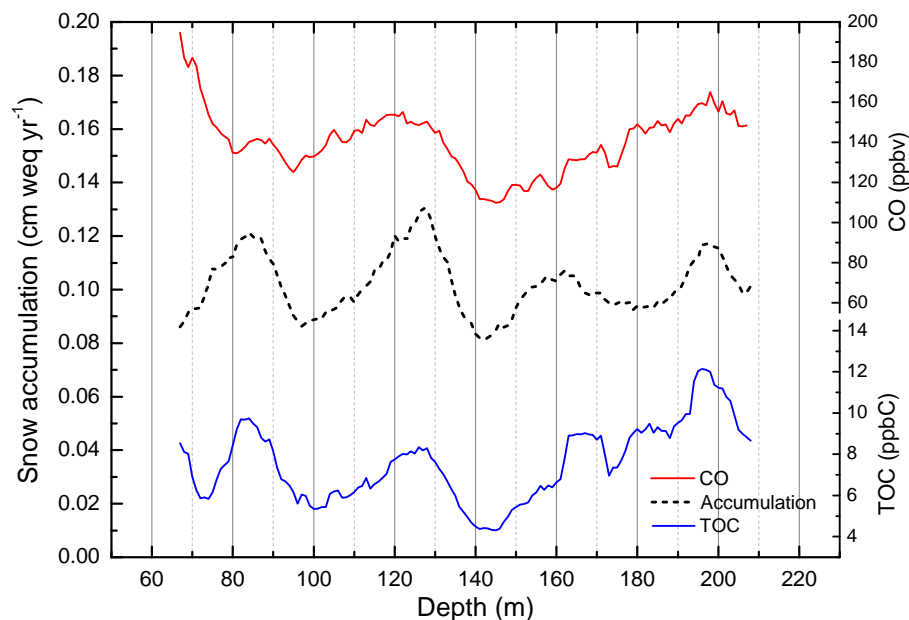
Figure 5. Running averages (10 m windows) of TOC and CO concentrations for the Tunu13 core, plotted along with annually averaged surface snow accumulation rate.

rates lower than $12 \, \mathrm{cm \, weq \, yr^{-1}}$. Ammonium remains when deposited due to acidic snow layers. In contrast to ammonium, formate evolves to a different form (presumably gaseous formic acid) that can partly be released into the free atmosphere above the snowpack or be remobilized to neighbouring winter layers. Such a process could contribute to explain lower TOC levels

445 observed under lower snow accumulation rates, and also the smoothed shape of the TOC peaks at Tunu13 (Fig. 4). This process can also promote in situ CO production in winter layers where some organic substrates can be remobilized.

3.3.3 Summary

Investigating the CO and TOC PLACE records did not reveal any evidence that the CO baseline could be influenced by in situ production at that site. In contrast, Tunu13 has a lower snow accumulation rate than other sites (Table 1) and thus the

450 analytical CFA smoothing of its CO record is more pronounced. This effect likely introduces a positive bias into the Tunu CO baseline record for ice sections impacted by in situ production, with some of the CO baseline signal likely incorporating in situ produced CO from summer ice layers. This limits the interpretation of Tunu13 baseline as an atmospheric signal in this study. While the mean CO mixing ratio is significantly correlated to the mean TOC concentrations in ice at Tunu13, this is not the case for baseline CO level which does not exhibit significant correlations with mean or baseline TOC concentrations. But

455 we can not rule out that a redistribution of organic carbon along depth driven by OC post-deposition process (shifting the ammonium-formate equilibrium with the gas phase) impacts specifically the Tunu13 CO record by providing some additional organic substrates in winter layers.

3.4 Comparison of PLACE and Eurocore datasets

Haan et al. (1996, 1998) published a pioneering CO dataset based on discrete sampling of the Eurocore ice core. This dataset
460   revealed a smoothed CO signal, interpreted as not being affected by in situ production over the last 300 yrs (26 samples, depth range: 78-154 m). However, Haan et al.'s CO data for the period preceding 1700 CE displayed a relatively elevated and scattered signal with levels fluctuating from 90 to 180 ppbv, likely impacted by in situ production. Through our study, we were unable to identify a Greenland site where the ice archive provides a low and stable CO record similar to Haan et al.'s over the last few centuries. Specifically, the CO record retrieved from the PLACE ice-core, which was drilled less than 1 km away from
465   the Eurocore borehole, shows high frequency variability along the entire CFA record (80-153 m depth), and this observation is supported by discrete measurements conducted on the PLACE core with an analytical process in principle similar to the one deployed by Haan et al. (Sect. 2.2.6) (Fig. 6).
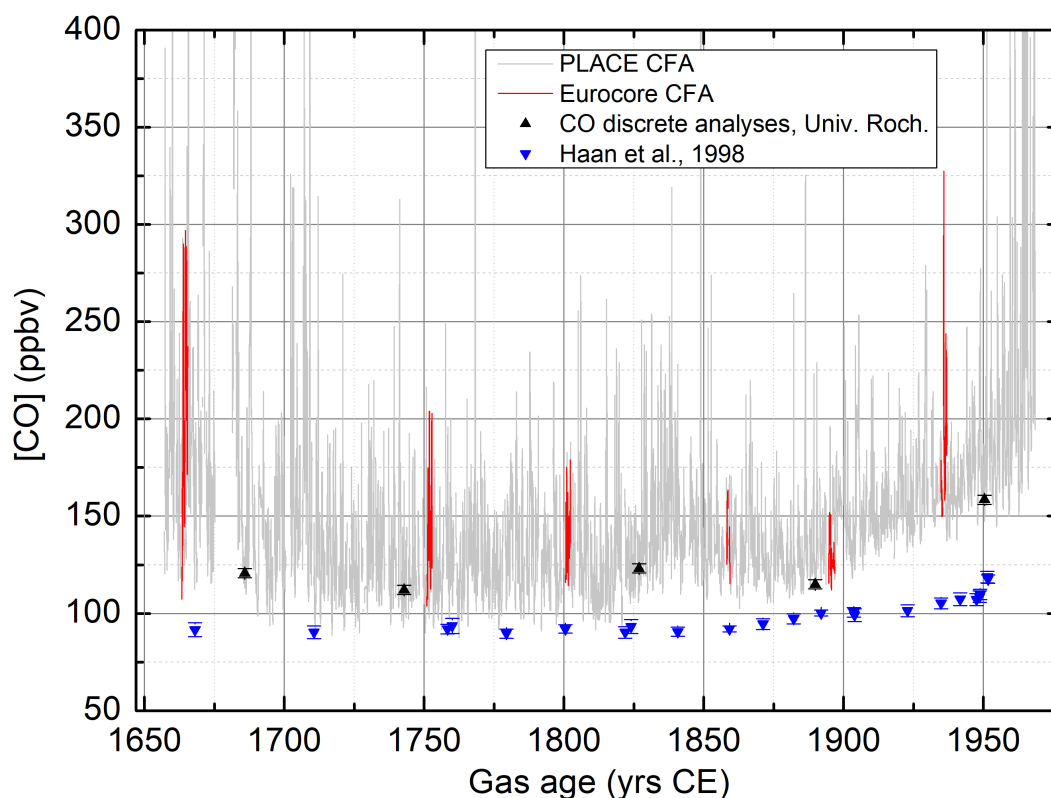
Figure 6. CO mixing ratio collected (i) along the Place ice core: continuous IGE CFA record, with 5th percentile baseline (black line), and discrete dataset (green dot); (ii) along the Eurocore archive : historical Eurocore discrete CO data (blue dot, Haan et al 1998), and CFA-based dataset measured in 2019 at IGE (red).

Over the 1700-1900 CE period, Eurocore discrete CO data are about 10 ppbv lower than the baseline of the PLACE CFA-based record (Figs. 6 and S23). Furthermore, the trend and rate of change of the two records are similar from 1700 to 1905

470 CE period but diverge over the 1925-1950 CE interval, with an increasing offset between datasets, and a sharp increase in CO concentrations observed only in the Eurocore record for the 1935-1950 CE time period.

To further investigate this apparent offset between our new Greenland CO records and the Eurocore CO record of Haan et al., we analysed six 50 cm-long sections of the 1989 Eurocore ice core with the gas CFA IGE setup in January 2019, at depths spanning 84 to 153 m. A fraction of the Eurocore core has been stored as an archive for 30 yrs at -20°C. We were able to
475 sample the Eurocore archive at exactly the same depths that Haan et al. did in the 1990s (the gaps left by the discrete sampling conducted by Haan and colleagues could be seen). Figure 6 shows Eurocore data (both from Haan et al. and our new CFA dataset), along with the PLACE IGE CFA record: to do so, an offset of +6 m was applied to the Eurocore depth scale, so as to take into account 26 yrs of snow accumulation that occurred between the Eurocore and PLACE drillings. Our CFA-based CO analyses reveal high variability along the Eurocore archive. We systematically observed higher CO mixing ratios
480 than previously reported by (Haan and Raynaud, 1998) including at the exact depths sampled by them. We established that such discrepancies were not related to differences in CO calibration scales by reanalyzing in 2015 the standard gases used by Haan el al. for calibrating their Eurocore dataset in the 90s. Overall, our CFA-based Eurocore data are in contradiction with the historical Eurocore dataset but are in good agreement with the PLACE record, in terms of both absolute levels and high variability. The discrete PLACE CO data, measured with a methodology similar to the one applied by Haan et al., also exhibit
485 higher values than Haan et al. dataset (Fig. 6), while they show an excellent agreement with the CFA CO dataset (Fig. S7).

To summarize, we have not been able to reconcile the historical Eurocore dataset of Haan et al. with a new Greenland ice-core CO dataset (PLACE). This is despite analysis of remaining Eurocore ice from depths co-located with the published Haan data and the fact that PLACE ice core was collected just 1 km away from Eurocore. The reasons for the relatively low and stable CO measurements reported in the 1990s for the Eurocore ice core remain unknown and our results bring the validity of the
490 Haan et al. (1996, 1995) results into question.

3.5 Constraining past atmospheric CO in the northern hemisphere

3.5.1 CO baseline records over the last 300 yrs

Extracting atmospheric information from a single CO record retrieved from a Greenland ice archive affected by in situ production features is challenging (e.g., Faïn et al., 2014). However, we show here that the PLACE, NGRIP, NEEM, and D4 records,
495 reconstructed from ice archives originating from different Greenland locations and drilled over a time period spanning more than a decade, exhibit common patterns. We conservatively exclude Tunu13 from paleoatmospheric interpretations, knowing that the Tunu13 baseline CO record could be positively bias by analytical smoothing or redistribution of organic carbon along depth (see Sect. 3.3). Fig. 1 reports 5th percentile CO baselines extracted over the last 300 years from the D4, NGRIP, NEEM, and PLACE records (DRI dataset). The four CO baseline records all lie within an envelope of maximum 20 ppbv range. From
500 1700 to 1875 CE, the records reveal stable or slightly increasing values remaining in the 100-115 ppbv range. From 1875 to 1950 CE, the records indicate a monotonic increase from 100-120 ppbv to 135-150 ppbv (i.e., a mean rate of increase of ~ 0.3 ppbv yr^{-1}). Interestingly, in 1835 CE, PLACE, NGRIP, NEEM, and D4 baselines exhibit a common maximum in CO

concentration but at a level just slightly higher than concentrations observed during the 1700-1820 CE period.

A multisite composite CO baseline spanning 1700-1957 CE was generated by considering D4, NEEM, NGRIP, and PLACE records and excluding Tunu13. For consistency, we only consider CO records collected on the same CFA gas setup (DRI). The multisite composite, reported in Fig. 7, was obtained by averaging CO baselines values interpolated on a common gas age scale. An uncertainty envelope (1σ) obtained by considering the independent uncertainty of individual records is plotted along with the composite. Overall, Fig. 7 reports a $\sim 30\%$ increase in CO concentration at high latitudes of the northern hemisphere atmosphere from pre-industrial to 1950 CE.
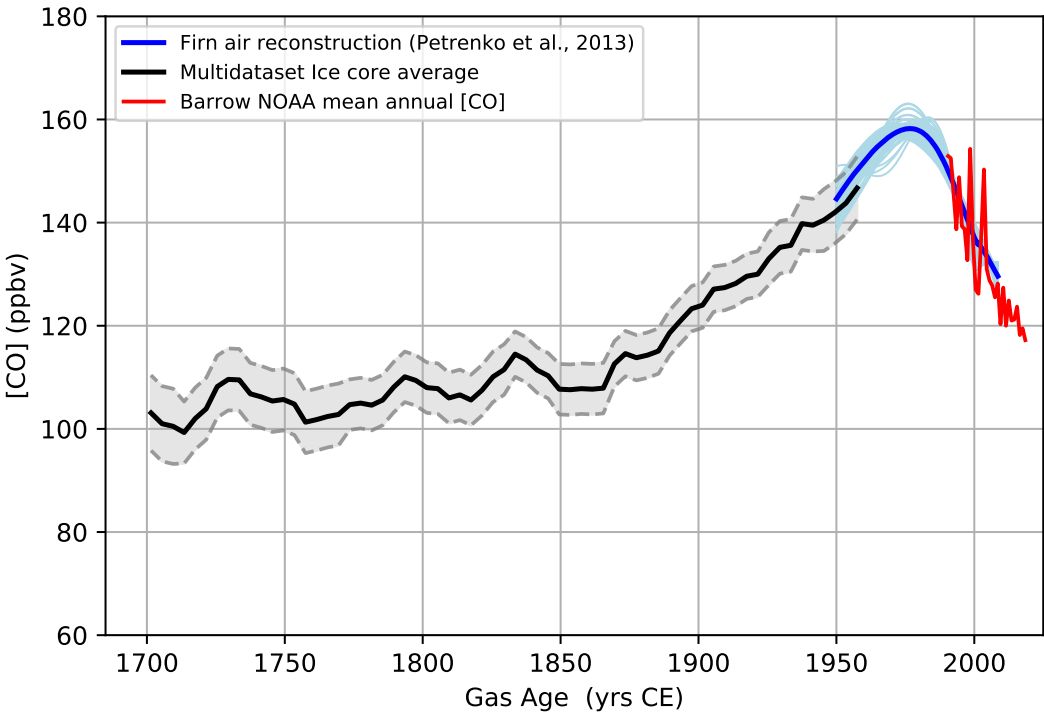
Figure 7. Past atmospheric CO mixing ratios for the Northern Hemisphere high latitudes and spanning 1700-2018 CE. Black line : multisite average obtained by combining baselines (5th percentiles) of continuous CO records collected at four Greenland sites (PLACE, NEEM, NGRIP and D4), representing an upper bound estimate of past atmospheric CO levels. Light blue : firn air records obtained by combining samples from NEEM, NGRIP, and Summit; blue : average firn air record (Petrenko et al., 2013) ; Red line : NOAA atmospheric monitoring at Barrow (Alaska, USA).

The fact that the CO baseline records from the four different Greenland ice cores are so consistent gives us confidence that our multisite reconstruction provides a reliable reconstruction of past atmospheric changes. An additional argument for that conclusion comes from the good overlap between our multisite reconstruction and CO data from firn air Greenland measurements

(section 3.5.2). However, we cannot exclude the possibility that past atmospheric CO levels could have been lower than shown in Fig. 7 and recommend that our multisite average should be taken as an upper bound of past atmospheric CO levels. If in situ

515 CO production drives the high frequency variability seen throughout the CFA records of these four ice cores, as we hypothesize (see Sect. 3.2), it is impossible to exclude the possibility that minimum CO levels may also be slightly affected (Sect 3.3).

3.5.2 Comparison with firn air reconstruction

An independent means to assess the validity of our atmospheric CO reconstruction is to compare it with a reconstruction of northern hemisphere high-latitude atmospheric CO mixing ratios from Greenland firn air, available for the period 1950-2008

520 CE (Petrenko et al., 2013). This reconstruction includes air samples collected in the open porosity of the firn at three sites in Greenland (NGRIP in 2001, Summit in 2006, and NEEM in 2008), and shows that CO records from these three sites agree well with each other as well as with recent atmospheric measurements from Barrow, Alaska. However, a small contribution from in situ CO production (up to 5 ppbv) within the firn open porosity itself could not be ruled out (Petrenko et al., 2013). This implies that the in situ CO production observed in ice core records which exhibit [CO] enhancement much larger than 5 ppbv

525 (Fig. 1) is a process happening within the ice matrix, after bubble closure. The reconstructed firn air history suggests that Arctic CO mixing ratio in 1950 CE was 138–148 ppbv, rose by 10–15 ppbv from 1950 to the 1970s, peaked in the 1970s or early 1980s, and finally declined by about 30 ppbv to present-day levels. The average firn air-based CO history spanning the last six decades (Petrenko et al., 2013) is shown on Fig. 7 along with our ice core CO composite reconstruction. The uncertainty in this scenario is captured by the variability of a set of 61 possible scenarios (Petrenko et al., 2013), and is shown as an envelope

530 on Fig. 7.

PLACE and D4 high resolution CO baseline records overlap with the firn record. The firn air data suggest that CO concentration spanned 138-148 ppbv in 1950 CE for the Arctic atmosphere Fig. 7). The 1950 CE CO concentration range as defined by PLACE and D4 baselines is 135-150 ppbv, indicating good agreement between firn air and ice core reconstructions.

3.5.3 Spatial representativity of the record

535 The Atmospheric Chemistry and Climate Model Intercomparison Project (ACCMIP; Lamarque et al., 2013) investigated the long-term changes in atmospheric composition between 1850 and 2100, with the goal of documenting atmospheric composition changes. To investigate the spatial representativity of the ice core record, we compared the CO mixing ratios simulated in the frame of the ACCMIP exercice for the years 1980 and 2000 and averaged over three different areas: the 45-90°N latitudinal band, an area encompassing the Greenland ice sheet (20-60°W; 60-84°N), and the single grid point including the PLACE

540 drilling location. Average [CO] over Greenland and [CO] at the PLACE drilling location are identical. However, atmospheric [CO] simulated for the 45-90°N latitudinal band is about 12% higher than [CO] simulated over Greenland. These results support our approach to combine ice core reconstructions obtained from different Greenlandic locations, but indicate that the absolute CO concentrations derived from our datasets are representative of the Greenlandic, Arctic, atmosphere, and may underestimate the average CO concentrations for the entire 45-90°N latitudinal band. On the other hand, the temporal changes depicted by

545 our composite record probably have a larger spatial significance than the Greenlandic context alone.

4 Summary and conclusions

New continuous profiles of CO mixing ratio have been measured along five Greenlandic ice cores, the PLACE, NGRIP, D4, Tunu13 and NEEM-SC archives. We also revisited the NEEM-2011-S1 dataset (Faïn et al., 2014). By coupling ice core melter systems with online measurements (SARA spectrometer), 700 m of ice were analyzed at high resolution for CO mixing ratio. This methodology has greatly improved over the last decade, with excellent external precision, low and well-constrained blank values, and a good accuracy. All investigated records revealed high and variable concentrations that can not be interpreted as changes in atmospheric CO, but are most likely related to in situ production occurring within the ice archives themselves after bubble closure. Additional measurements conducted on individual discrete samples allowed us to rule out the possibility of rapid CO production from organics in the ice during melting or other large CFA system artifacts. We have not been able to reconcile the prior Eurocore dataset of Haan et al. (1996, 1998) with any of the new Greenland ice core CO measurements made by both discrete and continuous analytical methods. Our results therefore question the accuracy of the relatively low and stable CO values reported by Haan et al. (1996, 1998) for the Eurocore ice core.

We have presented a multisite average ice core reconstruction of past atmospheric CO for the northern hemisphere high latitudes, covering the period from 1700 to 1950 CE, providing an upper bound estimate of past atmospheric CO abundance. This signal of paleo-atmosphere was extracted from the low frequency variability of the CO records' baselines of the PLACE, D4, NEEM, and NGRIP archives which all exhibit consistent trends despite different surface accumulation snow rates and chemical compositions. From 1700 to 1875 CE, the multisite average record is stable with a slight increase with time from 103 to 114 ppbv. Our upper-bound value for CO mixing ratio at preindustrial times in the Arctic is 110 ppbv. From 1875 to 1950 CE, the CO increases monotonically from 114 to 142 ppbv, with a rate of increase of about 0.3 ppbv yr^{-1}. Finally, an excellent agreement between our ice core based record and previously published firn air reconstruction is observed in the 1950s (Petrenko et al., 2013). The ice-core and firn [CO] histories, spanning 1700-2010 CE, exhibit similar patterns to an up-to-date combined inventory of anthropogenic and open burning CO emissions (van Marle et al., 2017; Hoesley et al., 1998). Our CFA-based multisite Greenland ice core CO reconstruction provides an indication of the timing and magnitude of past variations in the high northern latitude CO burden that can provide a benchmark for future atmospheric chemistry model studies. Specifically, a natural extension of this work should be the comparison of our ice-core-based atmospheric CO reconstruction with model outputs from the AerChemMIP exercise (Collins et al., 2017).

Acknowledgements. This work was supported by the following programs: the French ANR projects RPD-COCLICO (#10-RPDOC-002-01, X.F.) and NEEM (#07-VULN-09-001), the EU grants FP7-IP #ENV-2010/265148 (project Pegasos, X.F.) and FP7 ERC #291062 (project Ice&Lasers, J.C.), the US NSF awards #1406236 (V.V.P.), #0221515 (J.R.M.), #0909541 (J.R.M.), #1204176 (J.R.M.), #1406219 (J.R.M.), and #0968391 (E.B., Partnerships in International Research and Education, project PIRE), the Packard Fellowship for Science and Engineering (V.V.P.), and finally the French national program LEFE/INSU (project GreenCO, X.F.). Grateful thanks go to Olivia Maselli, Larry Layman, Daniel Pasteris, Michael Sigl, and other members of the DRI team who assisted with the measurement campaigns. We thank Frederic Prié, Elise Fourre, and Amaelle Landais for their help in the continuous measurement of water isotopes along the PLACE core

at IGE, in 2017. We are grateful to Ray Langenfelds for the measurements of gas standards at CSIRO, in 2015. We thank Sophie Szopa
and Kostas Tsigaridis for our useful discussions. Polar Field Services and the 109th New York Air National Guard, and the French Polar
Institute (IPEV) provided logistical support for ice core drilling. We are grateful to drillers and field teams. The NEEM project is directed
by the Center for Ice and Climate at the Niels Bohr Institute, Copenhagen, and the US NSF OPP. It is supported by funding agencies and
institutions in Belgium (FNRS-CFB and FWO), Canada (NRCan/GSC), China (CAS), Denmark (FIST), France (IPEV, CNRS/INSU, CEA
and ANR), Germany (AWI), Iceland (RannIs), Japan (NIPR), Korea (KOPRI), The Netherlands (NWO/ALW), Sweden (VR), Switzerland
(SNF), United Kingdom (NERC), and the USA (US NSF, OPP). NGRIP is a multinational research program funded by participating insti-
tutions in Denmark, France, Germany, Japan, Sweden, Switzerland Belgium, Iceland, and the United States. This work also benefited from
data available in the public NOAA ESRL database. We thank the people involved in the acquiring, analysis and accessibility of these data.
This manuscript was largely improved by constructive reviews from Murat Aydin and Maria Elena Popa.

Data availability.   The high resolution carbon monoxide datasets are available on the PANGEA database.

Author contributions.   This scientific project was designed by XF, JC, VVP, RR, EB, and TB. The high resolution carbon monoxide mea-
surements were carried out by XF and RR, with support of KF, TB, JC and EB. Discrete CO analyses were carried out by PP and EC, and
chemistry analyses were carried out by NC and JRM. XF, PP, and VVP participated in the PLACE drilling. RR participated in the Tunu13
drilling. The codes for data processing and modelling were developed by KF, JRM, and XF. All authors contributed to the interpretation of
the data. The manuscript was written by XF with the help of all co-authors.

Competing interests.   The authors declare having no competing interests

References

Allan, D.: Statistics of atomic frequency standards, Proceedings of the IEEE, 54, 221–230, https://doi.org/10.1109/PROC.1966.4634, 1966.

Butler, J. H., Battle, M. O., Bender, M., Montzka, S. A., Clarke, A. D., Saltzman, E. S., M., S. C., Severinghaus, J., and Elkins, J. W.: A record of atmospheric halocarbons during the twentieth century from polar firn air, Nature, 399, 749–755, 1999.

Clark, I. D., Henderson, L., Chappellaz, J., Fisher, D., Koerner, R., Worthy, D. E. J., Kotzer, T., Norman, A. L., and Barnola, J. M.: CO2 isotopes as tracers of firn air diffusion and age in an Arctic ice cap with summer melting, Devon Island, Canada, Journal of Geophysical Research-Atmospheres, 112, https://doi.org/D01301 10.1029/2006jd007471, 2007.

Collins, W. J., Lamarque, J.-F., Schulz, M., Boucher, O., Eyring, V., Hegglin, M. I., Maycock, A., Myhre, G., Prather, M., Shindell, D., and Smith, S. J.: AerChemMIP: quantifying the effects of chemistry and aerosols in CMIP6, Geoscientific Model Development, 10, 585–607, https://doi.org/10.5194/gmd-10-585-2017, 2017.

community members, N.: High-resolution record of Northern Hemisphere climate extending into the last interglacial period, Nature, https://doi.org/10.1038/nature02805, 2004.

Conte, L., Szopa, S., Séférian, R., and Bopp, L.: The oceanic cycle of carbon monoxide and its emissions to the atmosphere, Biogeosciences, 16, 881–902, https://doi.org/10.5194/bg-16-881-2019, 2019.

Crutzen, P. J.: A discussion of the chemistry of some minor constituents in the stratosphere and troposphere, Pure and Applied Geophysics, 106-108, 1385–1399, https://doi.org/10.1007/BF00881092, 1973.

Deeter, M. N., Edwards, D. P., Francis, G. L., Gille, J. C., Martínez-Alonso, S., Worden, H. M., and Sweeney, C.: A climate-scale satellite record for carbon monoxide: the MOPITT Version 7 product, Atmospheric Measurement Techniques, 10, 2533–2555, https://doi.org/10.5194/amt-10-2533-2017, 2017.

Duncan, B., Logan, J. A., Bey, I., Megretskaia, I. A., Yantosca, R. M., Novelli, P. C., Jones, N. B., and Rinsland, C. P.: Global budget of CO, 1988-1997: Source estimates and validation with a global model, Journal of Geophysical Research-Atmospheres, 112, https://doi.org/10.1029/2007jd008459, 2007.

Faïn, X., Chappellaz, J., Rhodes, R. H., Stowasser, C., Blunier, T., McConnell, J. R., Brook, E. J., Preunkert, S., Legrand, M., Debois, T., and Romanini, D.: High resolution measurements of carbon monoxide along a late Holocene Greenland ice core: evidence for in situ production, Climate of the Past, 10, 987–1000, https://doi.org/10.5194/cp-10-987-2014, 2014.

Fourteau, K., Faïn, X., Martinerie, P., Landais, A., Ekaykin, A. A., Lipenkov, V. Y., and Chappellaz, J.: Analytical constraints on layered gas trapping and smoothing of atmospheric variability in ice under low-accumulation conditions, Climate of the Past, 13, 1815–1830, https://doi.org/10.5194/cp-13-1815-2017, 2017.

Gkinis, V., Popp, T. J., Blunier, T., Bigler, M., Schupbach, S., Kettner, E., Johnsen, S. J., and Schüpbach, S.: Water isotopic ratios from a continuously melted ice core sample, Atmospheric Measurement Techniques, 4, 2531–2542, https://doi.org/10.5194/amt-4-2531-2011, 2011.

Haan, D. and Raynaud, D.: Ice core record of CO variations during the last two millennia: atmospheric implications and chemical interactions within the Greenland ice, Tellus Series B-Chemical and Physical Meteorology, 50, 253–262, 1998.

Haan, D., Martinerie, P., and Raynaud, D.: Ice core data of atmospheric carbon monoxide over Antarctica and Greenland during the last 200 years, Geophysical Research Letters, 23, 2235–2238, 1996.

Haan, D., Zuo, Y., Gros, V., and Brenninkmeijer, C. A. M.: Photochemical production of carbon monoxide in snow, Journal of Atmospheric Chemistry, 40, 217–230, 2001.

Hagler, G. S. W., Bergin, M. H., Smith, E. a., Dibb, J. E., Anderson, C., and Steig, E. J.: Particulate and water-soluble carbon measured in recent snow at Summit, Greenland, Geophysical Research Letters, 34, https://doi.org/https://doi.org/10.1029/2007GL030110, 2007.

635 Hoesly, R. M., Smith, S. J., Feng, L., Klimont, Z., Janssens-Maenhout, G., Pitkanen, T., Seibert, J. J., Vu, L., Andres, R. J., Bolt, R. M., Bond, T. C., Dawidowski, L., Kholod, N., Kurokawa, J.-i., Li, M., Liu, L., Lu, Z., Moura, M. C. P., O'Rourke, P. R., and Zhang, Q.: Historical (1750–2014) anthropogenic emissions of reactive gases and aerosols from the Community Emissions Data System (CEDS), Geoscientific Model Development, 11, 369–408, https://doi.org/10.5194/gmd-11-369-2018, 2018.

Khalil, M., Pinto, J., and Shearer, M.: Atmospheric carbon monoxide, Chemosphere - Global Change Science, 1, ix–xi,
640 https://doi.org/10.1016/S1465-9972(99)00053-7, 1999.

Kuhl, T. W., Johnson, J. A., Shturmakov, A. J., Goetz, J. J., Gibson, C. J., and Lebar, D. A.: A new large-diameter ice-core drill: the Blue Ice Drill, Annals of Glaciology, 55, 1–6, https://doi.org/10.3189/2014AoG68A009, 2014.

Lamarque, J.-F., Shindell, D. T., Josse, B., Young, P. J., Cionni, I., Eyring, V., Bergmann, D., Cameron-Smith, P., Collins, W. J., Doherty, R., Dalsoren, S., Faluvegi, G., Folberth, G., Ghan, S. J., Horowitz, L. W., Lee, Y. H., MacKenzie, I. a., Nagashima, T., Naik, V., Plummer,
645 D., Righi, M., Rumbold, S. T., Schulz, M., Skeie, R. B., Stevenson, D. S., Strode, S., Sudo, K., Szopa, S., Voulgarakis, a., and Zeng, G.: The Atmospheric Chemistry and Climate Model Intercomparison Project (ACCMIP): overview and description of models, simulations and climate diagnostics, Geoscientific Model Development, 6, 179–206, https://doi.org/10.5194/gmd-6-179-2013, 2013.

Legrand, M. and De Angelis, M.: Light carboxylic acids in Greenland ice: A record of past forest fires and vegetation emissions from the boreal zone, Journal of Geophysical Research, 101, 4129, https://doi.org/10.1029/95JD03296, 1996.

650 Legrand, M. and Mayewski, P.: Glaciochemistry of polar ice cores: A review, REVIEWS OF GEOPHYSICS, 35, 219–243, 1997.

Legrand, M., McConnell, J. R., Fischer, H., Wolff, E. W., Preunkert, S., Arienzo, M., Chellman, N., Leuenberger, D., Maselli, O. J., Place, P., Sigl, M., Schupbach, S., and Flannigan, M.: Boreal fire records in Northern Hemisphere ice cores: A review, Climate of the Past, 12, 2033–2059, https://doi.org/10.5194/cp-12-2033-2016, 2016.

Lelieveld, J., Gromov, S., Pozzer, A., and Taraborrelli, D.: Global tropospheric hydroxyl distribution, budget and reactivity, Atmospheric
655 Chemistry and Physics, 16, 12 477–12 493, https://doi.org/10.5194/acp-16-12477-2016, 2016.

Maselli, O. J., Fritzsche, D., Layman, L., McConnell, J. R., and Meyer, H.: Comparison of water isotope-ratio determinations using two cavity ring-down instruments and classical mass spectrometry in continuous ice-core analysis., Isotopes in environmental and health studies, 49, 387–98, https://doi.org/10.1080/10256016.2013.781598, 2013.

McConnell, J. R. and Edwards, R.: Coal burning leaves toxic heavy metal legacy in the Arctic., Proceedings of the National Academy of
660 Sciences of the United States of America, 105, 12 140–12 144, https://doi.org/10.1073/pnas.0803564105, 2008.

McConnell, J. R., Lamorey, S., and Taylor, K. C.: Continuous ice-core chemical analyses using inductively coupled plasma mass spectrometry, Environmental Science and Technology, 36, 7–11, 2002.

McConnell, J. R., Edwards, R., Kok, G. L., Flanner, M. G., Zender, C. S., Saltzman, E. S., Banta, J. R., Pasteris, D. R., Carter, M. M., and Kahl, J. D. W.: 20th-century industrial black carbon emissions altered arctic climate forcing, Science, 317, 1381–1384, 2007.

665 Morville, J., Kassi, S., Chenevier, M., and Romanini, D.: Fast, low-noise, mode-by-mode, cavity-enhanced absorption spectroscopy by diode-laser self-locking, Applied Physics B-Lasers and Optics, 80, 1027–1038, https://doi.org/10.1007/s00340-005-1828-z, 2005.

NEEM community members: Eemian interglacial reconstructed from a Greenland folded ice core, Nature, 493, 489, https://doi.org/10.1038/nature11789, 2012.

Novelli, P. C., Masarie, K. A., and Lang, P. M.: Distributions and recent changes of carbon monoxide in the lower troposphere, Journal of
670 Geophysical Research, 103, 19 015–19 033, 1998.

Petrenko, V. V., Martinerie, P., Novelli, P. C., Etheridge, D. M., Levin, I., Wang, Z., Blunier, T., Chappellaz, J., Kaiser, J., Lang, P., Steele, L. P., Hammer, S., Mak, J., Langenfelds, R. L., Schwander, J., Severinghaus, J., Witrant, E., Petron, G., Battle, M. O., Forster, G., Sturges, W. T., Lamarque, J.-F., Steffen, K., and White, J. W. C.: A 60 yr record of atmospheric carbon monoxide reconstructed from Greenland firn air, Atmospheric Chemistry and Physics, 13, 7567–7585, https://doi.org/10.5194/acp-13-7567-2013, 2013.

675 Rhodes, R. H., Faïn, X., Stowasser, C., Blunier, T., Chappellaz, J., McConnell, J. R., Romanini, D., Mitchell, L. E., and Brook, E. J.: Continuous methane measurements from a late Holocene Greenland ice core: Atmospheric and in-situ signals, Earth and Planetary Science Letters, 368, 9–19, https://doi.org/10.1016/j.epsl.2013.02.034, 2013.

Rhodes, R. H., Brook, E. J., Chiang, J. C. H., Blunier, T., Maselli, O. J., McConnell, J. R., Romanini, D., and Severing-haus, J.: Enhanced tropical methane production in response to iceberg discharge in the North Atlantic, Science, 348, 1016–9,
680 https://doi.org/10.1126/science.1262005, 2015.

Rhodes, R. H., Faïn, X., Brook, E. J., McConnell, J. R., Maselli, O. J., Sigl, M., Edwards, J. S., Buizert, C., Blunier, T., Chappellaz, J., and Freitag, J.: Local artifacts in ice core methane records caused by layered bubble trapping and in situ production: a multi-site investigation, Climate of the Past, 12, 1061–1077, https://doi.org/10.5194/cp-12-1061-2016, 2016.

Schwander, J. and Rufli, H.: Electromechanical drilling of a 300-m core in a dry hole at Summit, Mem. Natl Inst, Polar Res, 49, 93–94, 1994.

685 Stowasser, C., Buizert, C., Gkinis, V., Chappellaz, J., Schüpbach, S., Bigler, M., Faïn, X., Sperlich, P., Baumgartner, M., Schilt, a., Blunier, T., and Schupbach, S.: Continuous measurements of methane mixing ratios from ice cores, Atmospheric Measurement Techniques, 5, 999–1013, https://doi.org/10.5194/amt-5-999-2012, 2012.

van der Werf, G. R., Randerson, J. T., Giglio, L., van Leeuwen, T. T., Chen, Y., Rogers, B. M., Mu, M., van Marle, M., Morton, D. C., Collatz, G. J., Yokelson, R. J., and Kasibhatla, P. S.: Global fire emissions estimates during 1997–2016, Earth System Science Data, 9, 697–720,
690 https://doi.org/10.5194/essd-9-697-2017, 2017.

Wang, Z., Chappellaz, J., Martinerie, P., Park, K., Petrenko, V. V., Witrant, E., Emmons, L. K., Blunier, T., Brenninkmeijer, C. A. M., and Mak, J.: The isotopic record of Northern Hemisphere atmospheric carbon monoxide since 1950: implications for the CO budget, Atmospheric Chemistry and Physics, 12, 4365–4377, https://doi.org/10.5194/acp-12-4365-2012, 2012.

Zheng, B., Chevallier, F., Yin, Y., Ciais, P., Fortems-Cheiney, A., Deeter, M. N., Parker, R. J., Wang, Y., Worden, H. M., and Zhao, Y.: Global
695 atmospheric carbon monoxide budget 2000–2017 inferred from multi-species atmospheric inversions, Earth System Science Data, 11, 1411–1436, https://doi.org/10.5194/essd-11-1411-2019, 2019.

1 **Supplementary Information**

2 **Northern Hemisphere atmospheric history of carbon monoxide since**

3 **preindustrial times reconstructed from multiple Greenland ice cores**

4 **Xavier Faïn et al. (2021), Climate of the Past**

5 **Summary**

1. Methodology

1.1. Location of drillings

Figure S1. Drilling locations of the ice cores featured in this study: NEEM, Tunu13, NGRIP, D4, PLACE. These sites are all located within Greenland.

1.2. Ice core chronologies

Ice core	Δage (yrs)	FWHM (yrs)	Ice Age Scale	Gas Age Scale
D4	90	14	ALC+VS Gas	Tied to WDC06A-7[b] & Law Dome[c]
Tunu13	314-369	21-27	ALC+Vs[d]	Tied to WDC06A-7[b]
NGRIP	235	18	Ice: GICC05[e]	Tied to WDC06A-7[b]
PLACE	195	n.d.	ALC+VS	Tied to WDC06A-7[b]
NEEM-SC	187[d]	17	Ice: GICC05[e]	Gas: GICC05[e]
NEEM-2011-S1	187[d]	17	Ice: GICC05[e]	Gas: GICC05[e]

Notes: Δage=difference between gas age and ice age. If no reference is provided, value is estimated by age scale synchronisation; FWHM=Full Width at Half Maximum of gas age distribution at close-off depth estimated by OSU firn air model (Rosen et al., 2014); ALC=annual layer count; VS=volcanic synchronisation; gas age scales do not incorporate lock-in zone measurements. [a] Buizert et al. (2014); [b] Mitchell et al. (2013); [c] MacFarling Meure et al. (2006); [d] Sigl et al. (2015); [e] Rasmussen et al. (2013).

Table S1. Information on ice and gas age scales for the ice cores featured in this study

Faïn et al., 2021, CP, Supplementary Information

1.3. Differences and similarities between DRI and IGE CFA setups

Specific details of analytical setups are reported in Table S2. Small operational differences exist between the laboratory setups at DRI and IGE. First, DRI and IGE melter geometries are different, and described by McConnell et al. (2002) for DRI, and Bigler et al. (2011) for IGE. Second, the melting rate was higher at DRI compared to IGE ([5-6] cm min^{-1} and 4 cm min^{-1}, respectively). Finally, DRI and IGE debubblers have different geometry. DRI debubbler (Plexiglas-made) allows for ultra-high resolution of liquid phase analyses, but results in a larger mixing of the gas phase sample compared to the IGE debubbler (glass-made) specifically designed for gas measurement.

The same optical feedback cavity enhanced absorption spectrometer was used to analyse carbon monoxide and methane at both DRI and IGE and during the all analytical campaigns (2013, 2015, and 2017). The same instrument was used by Faïn et al. (2014) for measurements of the NEEM-2011-S1 core in 2011 at DRI.

Two different gas extraction units were used (i) in 2013 (DRI), and (ii) both in 2015 at DRI and 2017 at IGE, respectively. A gas extraction unit includes a degasser, a pressure transducer, a 6-ways valve, and a homemade Nafion dryer (Fig.1 of Rhodes et al., 2013). Improvements on the design and operation of this unit largely explain the improved stability of the [CO] CFA signal, as shown by the much larger optimal IT values observed for the 2015 and 2017 campaigns (Table S2).

Finally, the D4, Tunu13, and a fraction of the NEEM-SC cores were analysed with a Micromodule 0.5×1 degasser (Membrana GmbH, Germany). Other cores were analyzed with an Idex Transfer-Line degasser instead.

Faïn et al., 2021, CP, Supplementary Information

Ice core	Laboratory of analysis	Analysis date	Depth Interval (m)	Mean melting rate (cm min-1)	Mean gas sample flow (sccm min-1)	Melter head	Degasser	Optimal Integration Time (s)	Integration Time applied (s)	Internal precision at IT (ppbv) (2σ)	External precision (ppbv)	System response time (min)	CO blank (ppbv)	CO solubility losses (%)
Tumu13	DRI	13-21/08/13	213–73	5.9	1.8	Standard	M	130	6	1.4	5.7	15	35±7	3.7%
D4	DRI	7-9/08/13	146–61	7.6	1.5	Small	M	130	6	1.4	5.7	15	35±7	3.7%
		15/08/2013	145–123	7.6	1.5	Small	M	130	6	1.4	5.7	15	35±7	3.7%
NEEM-SC	DRI	3-6/09/13	573–491, 444–399	5.7	1.9	Standard	M	130	6	1.4	5.7	15	35±7	3.7%
		7-8/10/13	491–444	5.7	1.8	Standard	IL	130	6	1.4	6.6	14.2	12.6±4.4	6.0%
NGRIP	DRI	08/31/13	91–74			Standard	IL	130	6	1.4	6.6	14.2	12.6±4.4	6.0%
		30/09-4/10/13	254–207, 108–91, 569–519	5.7	1.4	Dual ring	IL	130	6	1.4		14.2	12.6±4.4	6.0%
PLACE	DRI	28/09-01/10/15	153 - 80	5.4	1.6	Standard	IL	>500	1	1.6	6.6	9.3	7.4±1.4	6.4%
PLACE	IGE	31/01-10/02/17	153 - 80	4.0	1.4	Bigler et al., 2011	IL	>1000	1	1.2	3.3	1.6	4.1±1.2	8.8%

Degasser: M=Membrana Liqui-cel Micromodule; IL=Idex Transfer Line degasser.

Melter head; three different styles were used: standard = as McConnell et al. (2002); small = smaller cross-sectional area; dual ring = new design with two concentric sample rings available for gas

Table S2. CFA setup specifications and performances of the different analytical campaigns.

Faïn et al., 2021, CP, Supplementary Information

1 **1.4. Calibration of SARA analyser**

2 The optical response of OF-CEAS (based on absorption) to gaseous concentrations of samples
3 circulating in the cavity of the spectrometer is highly linear (Morville 2005). Such linearity has been
4 previously reported for concentrations ranging over more than three decades for methane (e.g.,
5 Fourteau et al., 2017).

6 Similarly, we observed a highly linear relationship of our OF-CEAS spectrometer when measuring
7 CO mixing ratios over a [0-100 ppbv] range. Such linearity was demonstrated by a dilution
8 experiment conducted by mixing a 100 ppbv standard gases and CO - Air Zero with two MFC
9 MKS recently calibrated (concentrations ranging [0-100] ppbv could thus be generated). Fig. S2
10 reports uncalibrated SARA [CO] plotted along expected [CO] based on dilution flows, with a
11 negligible offset and a 0.92 slope. Recent laboratory measurements have extended the
12 observation of the OF-CEAS linearity at CO concentrations of 2.7 ppmv (R. Grilli, pers. com.).
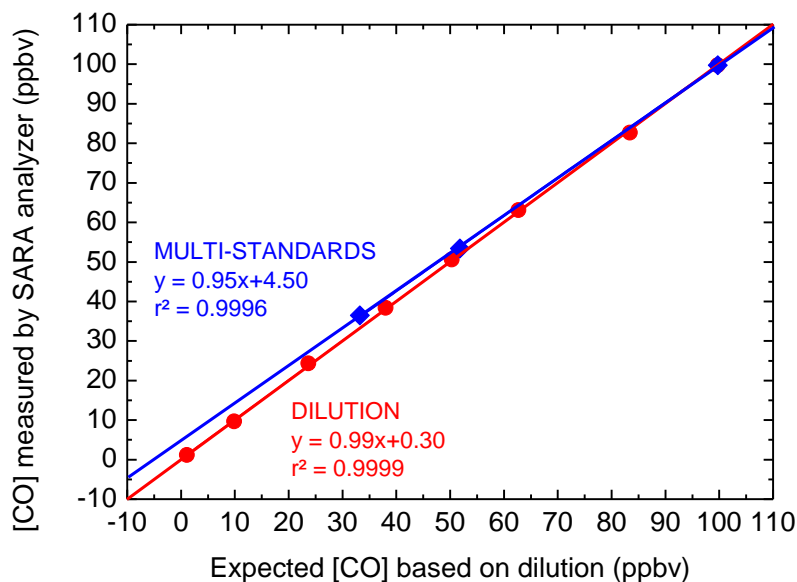
14 **Figure S2.** Calibrations of the OF-CEAS SARA analyzer for CO. (i) multi-standard calibrations (blue dots):
15 uncalibrated SARA CO is plotted along with NOAA WMO_2014 CO concentrations from three standard
16 gases. (ii) a dilution experiment conducted by mixing a 100 ppbv standard gas and CO-Air Zero with two
17 mass flow controllers: uncalibrated SARA [CO] is plotted along with expected [CO] based on dilution flows.

Faïn et al., 2021, CP, Supplementary Information

1 For each analytical campaign, the OF-CEAS spectrometer was carefully calibrated on dry gas by

2 direct injection of a synthetic standard gas (Scott Marin, artificial gas mixtures) precisely calibrated

3 onto the NOAA/WMO X2014 scale, with a concentration close or above 100 ppbv (Table S3).

4 Knowing the excellent linearity of the instrument, a calibration factor was established as the ratio

5 of the NOAA-certified and the measured CO concentrations for this single standard gas. This is

6 consistent with the fact that the zero of the spectral measurements is intrinsically accurate.

Analytical campaign	Gas Cylinder used for OF-CEAS (SARA) calibration	Gas Cylinders used for CFA calibration	NOAA certified [CO] (ppbv)
DRI 2013		CA04382	56.6 ± 3.4
		CA04332	97.2 ± 0.0
	CC302559	CC302559	142.6 ± 0.1
DRI 2015		CB10010	57.9 ± 0.4
	CA04332	CA04332	97.2 ± 0.1
DRI 2013		CB09754	32.5 ± 0.1
		CB09722	51.7 ± 0.1
	CB09752	CB09752	100.1 ± 0.1

8 **Table S3.** Synthetic standard gases (Scott Marin, artificial gas mixtures) precisely calibrated onto the

9 NOAA/WMO X2014 scale and used for OF-CEAS and CFA calibrations.

11 1.5. Determination of CO CFA blank

12 Excellent agreement between replicate measurements conducted days apart, before blank

13 correction, suggests that CO blanks of gas-CFA analytical systems (both DRI and IGE) can be

14 very constant during an analytical campaign (Fig. S3; see Fig. 2 of Faïn et al., 2014). However,

15 how to quantify exactly such procedural blanks remains complex. Two approaches investigate

16 gas-CFA procedural blanks: single-standard measurements, or multi-standards calibration.

17 To evaluate CO blank with single-standard measurements approach, deionized (DI) water is

18 bubbled with a specific gas standard for at least 12 hours in a 2 liters reservoir, and this water is

19 later mixed with the same gas standard in the calibration loop (CL, section 2.2.2 of manuscript).

20 The positive offset between direct measurements of the dry gas standard with the spectrometer

21 and the CL measurements as described previously will directly indicate the procedural blank.

22 Single-standard measurements were conducted to evaluate CO blank of the IGE CFA setup. An

23 example of such experiment is as follow: DI water bubbled during 18 hours with a 58.7±0.3 ppbv

24 (NOAA/WMO X2014 scale) CO standard gas. The same standard gas was then mixed with this

Faïn et al., 2021, CP, Supplementary Information

1   DI water within the IGE calibration Loop, and circulated toward the degasser. CO mixing ratios of

2   62.8±0.5 ppbv is measured. A procedural CO blank of 4.1±0.6 ppbv is thus observed.
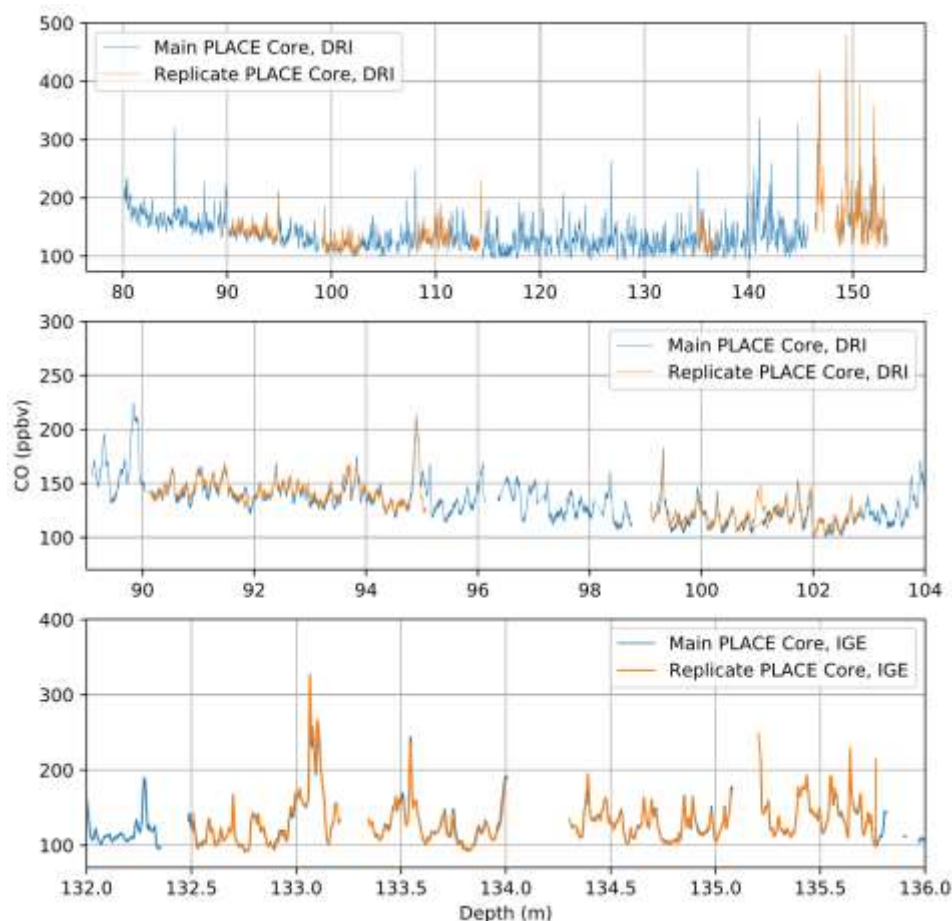
4   **Figure S3.** Replicate measurements of CO mixing ratios (Main cuts blue, Replicate cuts in orange)

5   conducted on the PLACE core (i) at DRI during the 2015 analytical campaign (upper and middle panels),

6   and (ii) at IGE during the 2017 analytical campaign (lower panel).

8   Multi-standard calibration loop datasets have been widely used before for methane (e.g., Rhodes

9   et al., 2016; Fourteau et al., 2017) and are obtained by mixing a range of standard gases of known

Faïn et al., 2021, CP, Supplementary Information

1 concentration with He-degassed DI water. The intercept observed when plotting expected versus

2 CL-determined concentrations reflects both the procedural blank and the fraction of gas remaining

3 in DI water after He-bubbling. Figure S4 reports multi-standards CO calibration obtained at DRI

4 in 2013 with both Micromodule and Transfer Line degassers, and the intercepts of 35 ppbv and

5 12.6 ppbv are the CO blank levels observed for these two specific CFA configurations. We applied

6 the multi-standards calibrations loop approach to evaluate CO blank for all continuous CO

7 datasets collected in this study (Table S2). At IGE, the multi-standards calibration provided an

8 Intercept for [CO] of 4.1 ppbv, in good agreement with the single-standard approach described

9 before. This good agreement demonstrates that the multi-standards calibration is a reliable

10 approach to evaluate CFA blank for gas of low solubility such as CO, i.e. the fraction of CO

11 remaining in DI water after He-bubbling is negligible. Estimation of the uncertainty of CO blanks

12 are reported on Table S2 and are based on repeated calibration loop measurements throughout

13 the campaigns (1σ).
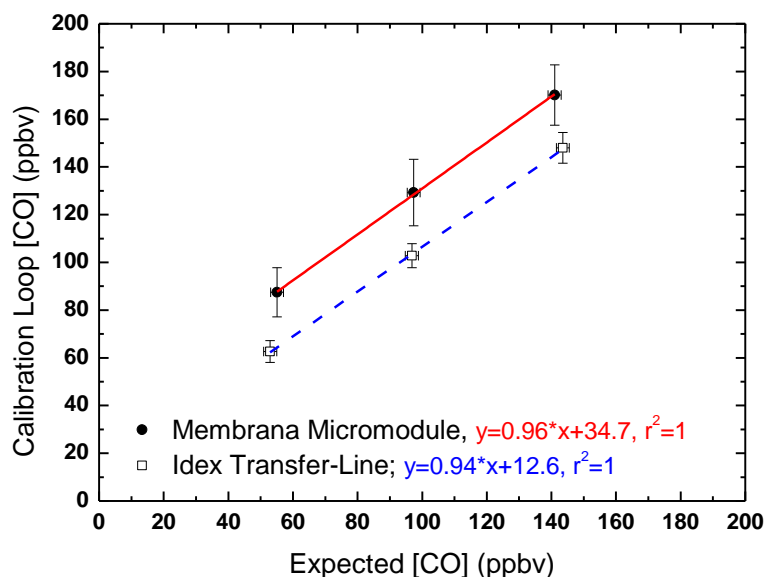
15 **Figure S4.** Multi-standards CO calibrations conducted at DRI in 2013 with both Micromodule and Transfer-

16 Line degassers.

Faïn et al., 2021, CP, Supplementary Information

1 Overall, using a Membrana MicroModule degasser results in larger CO blank, and we
2 consequently recommend the use of Idex Transfer-Line degassers for continuous CO analyses.
3 Also, any material (e.g., line, connections) should be carefully tested to assess potential CO
4 contamination. We have found that TEFZL is appropriate for CO analyses. Finally, CO blanks are
5 kept low by continuously running DI water through system lines during measurements periods.

7 1.6. Internal precision of CO CFA analyses

8 Internal precision and stability of gas-CFA measurements were evaluated by Allan variance tests
9 (Allan, 1966) applied to calibration loop dataset (DI degassed water mixed with a single standard
10 gas), and are reported on Fig. S5. Observed optimal integration times (i.e., time of lowest Allan
11 deviation) were 130 sec for the 2013 DRI campaign, larger than 500 sec for the 2015 DRI
12 campaign, and larger than 1000 sec for the IGE 2017 campaign. For the 2015 and 2017
13 campaigns, the design of the calibration loop (specifically, the volume of degassed water available
14 combined with the setup sample flow rate reproduce during calibration loop experiment) did not
15 allow a minimum in Allan Variance to be reached, but still provided an upper bound value.

16 To maximize the depth resolution, gas data are averaged over integration time (IT). Such
17 integration time was set up to 6 sec for the 2013 DRI campaign (Tunu13, D4, NGRIP, and NEEM-
18 SC ice cores), and 1 sec for the 2015 DRI and 2017 IGE campaigns (ice core : Place). The internal
19 precision (1σ) can be defined as twice the Allan deviation at these chosen integration times,
20 resulting in an internal precision of [CO] of 0.7 ppbv, 0.8 ppbv, 0.6 ppbv for the analytical
21 campaigns 2013-DRI, 2015-DRI, and 2017-IGE respectively.

Faïn et al., 2021, CP, Supplementary Information
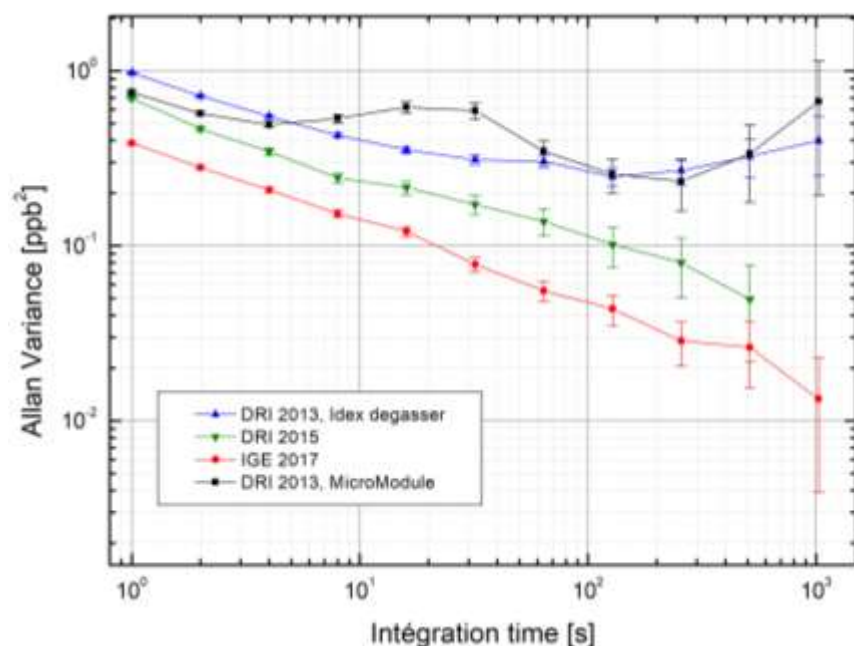
2 **Figure S5.** Allan variance results for calibration loop dataset (DI degassed water mixed with a single
3 standard gas) collected for the different CFA setup: DRI 2013 (both Transfer Line and Mircomodule
4 degassers), DRI 2015, and IGE 2017.

6 **1.7. External precision of CO CFA analyses**

7 External precision of the continuous CO measurements (i.e., including all sources of errors or
8 bias) can be investigated by melting replicate ice sticks on different days on a gas-CFA setup.
9 Specifically, we define the external precision as the pooled standard deviations calculated on the
10 differences of CO concentrations from main and replicate analysed ice sticks, averaging
11 continuous CO data over few cm long intervals. Specifically, after binning the main (M) data and
12 replicate (R) data into these few cm long intervals, we obtain n duplicate measurements. The
13 pooled standard deviation is then calculated as $\sqrt{\left(\left(\frac{\sum(M-R)^2}{2 \times n}\right)\right)}$.

14 For the DRI gas-CFA setup, an external precision of 5.7 ppbv can be extracted from a 18 m long
15 replicate section of the NEEM-2011-S1 core analyzed in 2011 (Faïn et al., 2014), averaged over

1   9 cm long intervals. In this study, we use this estimate of external precision to datasets collected

2   at DRI in 2013, with a Micromodule degasser (i.e., D4, Tunu13, a fraction of NEEM-SC).

3   Similar characterizations were conducted during the 2015 DRI and 2017 IGE analytical

4   campaigns by melting replicate sticks from the PLACE core, taking advantage of the large amount

5   of ice available (the PLACE core is 27 cm diameter, drilled with the Blue Ice Drill, see sect. 2.1 of

6   manuscript). 19.6 m (resp. 2.3 m) of replicate PLACE sticks were analysed at DRI in 2015 (at IGE

7   in 2017, resp.). Replicate sections of the PLACE core melted both at DRI and IGE are reported

8   on Fig. S3. CO concentrations measured on both main and replicate ice sticks were averaged by

9   binning over 196 10-cm long (resp., over 227 1-cm long) intervals at DRI (resp., at IGE). Figure

10   S6 reports an excellent correlation ($r2 = 0.99$; $p<0.01$) between averaged CO from main cuts

11   versus averaged CO from replicate cuts for both CFA setup. Finally, external precision of 6.6 ppbv

12   (resp., 3.3 ppbv) was calculated for the 2015 DRI campaign (resp., 2017 IGE campaign). In this

13   study, we apply the external precision value established for the 2015 DRI campaign is applied to

14   dataset collected at DRI in 2013 with a Transfer-Line degasser (i.e., a fraction of NEEM-SC and

15   NGRIP dataset).

Faïn et al., 2021, CP, Supplementary Information
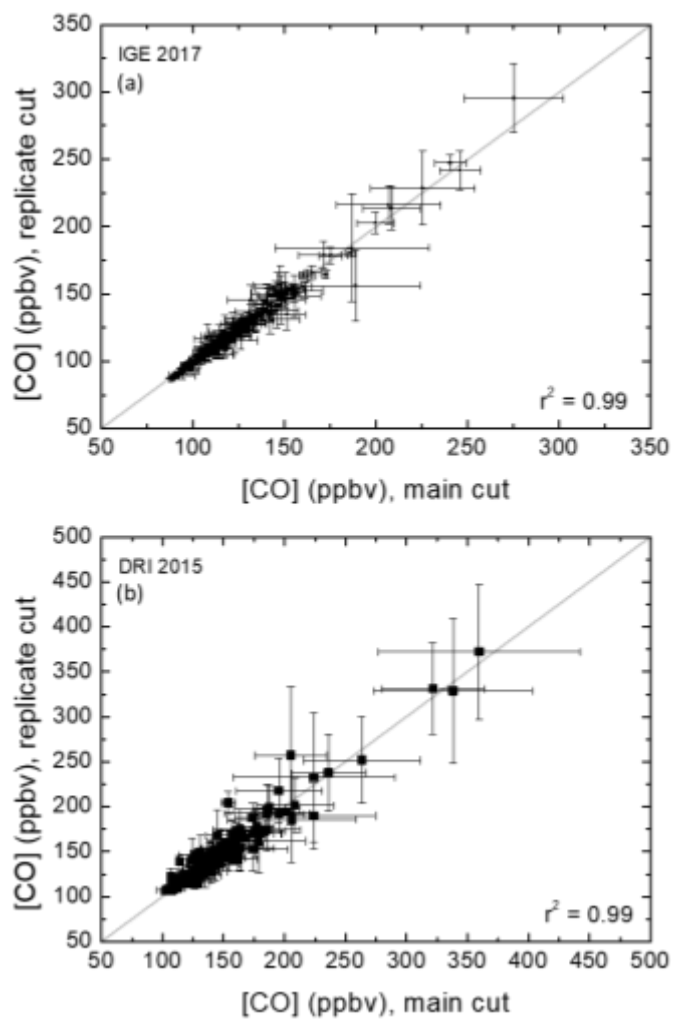
Figure S6. CO mixing ratios measured on both main and replicate PLACE ice sticks at DRI (a) and IGE

(b), after averaging data over 10-cm long (resp., over 1-cm long) intervals at DRI (resp., at IGE).

We are aware that longer replicate sections, spanning depths over the entire record, such as

conducted at DRI in 2015 (Fig. S3), can provide a more solid dataset for evaluating external

precision. We note that only the DRI PLACE dataset was used to extract atmospheric information

1 (section 3 of manuscript), notably because a more robust evaluation of the external precision was
2 available. However, the IGE dataset demonstrates that excellent precision of continuous CO
3 measurements is not limited to one specific setup, but rather achievable for all CFA laboratories.

1.8. Internal CO CFA calibration: improving accuracy

6 A fraction, or all, of gases dissolved in the water CFA sample flow are not recovered by the
7 degassers used in this study. CO solubility is higher than N2 or O2 solubility. This preferential
8 dissolution of CO in comparison to N2 and O2 results in underestimated CO mixing ratios when
9 detected at the gas outlet of the degasser. This underestimation of CO mixing ratios need to be
10 accurately quantified so as to provide an absolute calibration of CO continuous dataset. Henry's
11 Law theory suggests that temperature and gas/liquid ratio of the melted sample are two important
12 parameters influencing gas dissolution within the sample flow. Gas/liquid ratio of the melted
13 sample is likely related to the air content of the ice analysed, although this relationship may not
14 be straightforward (e.g., one cannot exclude losses of gas at the melter), and may differ with
15 melter geometry.

1.8.1. Rationale for an internal CFA calibration

17 In this study, we use the calibration loop so as to calibrate internally (i.e., with CFA data)
18 continuous CO datasets. This choice relies on the following observations:

19 ● The amount of gas dissolved in the water stream and not recovered by the degasser (Idex
20   Transfer-Line or Membrana Micromodule) is dependent on the CFA setup, i.e. dependent
21   on its geometry, components, operation. Consequently, a unique theoretical framework
22   cannot be applied to all dataset. Indeed, in this study a 73 m long ice core (PLACE) was
23   analysed on two different CFA setups (at IGE and DRI), for CO but also for methane
24   mixing ratios. This gas CFA laboratory intercomparison revealed that the fraction of
25   methane not recovered at IGE was larger than a DRI (10% and 13%, resp.). The gas
26   extraction unit (including an Idex Transfer-line degasser) and OFCEAS detection were
27   identical at DRI and IGE, pointing out that the melter and lines upstream the degasser can
28   result in different gas dissolution ratios.

29 ● To test further the influence of the CFA setup geometry and operation on gas dissolution
30   patterns, a series of 16 replicate 1m long ice sticks, all cut from the same Blue Ice Drill
31   (BID) large diameter core recovered in the vicinity of Greenland summit (C14 camp, Hmiel

Faïn et al., 2021, CP, Supplementary Information

1   et al., 2020), were melted at IGE in December, 2018, with varying operation and geometry
2   of the CFA setup. Each time, the fraction of methane not recovered was observed.
3   Specifically, the influence of following parameters on the preferential methane dissolution
4   were tested: melting speed (varying from 2.8 to 6 cm min^{-1}), sample flow (ranging 12 to 22
5   ml min^{-1}), melter geometry (geometry reported by Bigler et al., 2011, with inner sections
6   of 26 x 26 mm, or 24 x 24 mm), line lengths (adding 4 m long line sections in the system).
7   These tests are specific to the IGE setup, but they show: (i) no influence of the melting
8   speed, neither of the melter geometry, neither of the sample flow, on the preferential
9   methane dissolution. However, they reveal varying methane losses when changing line
10   geometry (up to 5% in mixing ratio).

11 Overall, these results show that CFA setups are dynamic systems, not at solubility equilibrium.

12 **1.8.2. Principle of calibration**

13 We hypothesize that CO and methane dissolution follow the same physical laws: consequently,
14 if a calibration loop (CL) is able to reproduce methane preferential dissolution, it should also
15 reproduce CO losses related to dissolution. Calibration loop is described in sections 2.2.2 of
16 manuscript and 1.5 of SI; briefly, a 10:90 mixture of synthetic air and degassed deionized (DI)
17 water can be introduced into the system via a 4-port valve located directly after the melterhead.
18 The water is sourced from a 2 L reservoir degassed by constantly bubbling ultra-pure helium
19 through it, and the fraction of He dissolved in DI water is later neglected. The air–water mixture
20 follows the same path through the system as the ice core sample before being analysed by the
21 laser spectrometer. We verified that no CO or CH4 specific fractionations occur at the degasser,
22 which would invalidate the previous hypothesis. To do so, we run consecutively the calibration
23 loop in two configurations: (i) with a degasser, and (ii) with an open split debubbler where gases
24 are transferred to the OF-CEAS analyzer without going through a membrane. Same CH4 and CO
25 mixing ratios were observed in both configurations. Finally, considering that gas dissolution within
26 the CFA setup is likely to vary with ice air content (AC), we tried to determine a specific calibration
27 for each ice core analyzed.

28 We first needed an estimation of methane losses related to dissolution, independent of the
29 calibration loop, from each ice core analyzed. For the archives Tunu13, D4 and NEEM,
30 preferential methane dissolution was already known (Rhodes et al., 2013, 2016). For the PLACE
31 and NGRIP archives, it was evaluated by direct comparison of CFA dataset with GISP2 discrete
32 record (Mitchell et al., 2013).

Faïn et al., 2021, CP, Supplementary Information

1 Then, liquid and gas flows injected through the calibration loop were chosen to reproduce ice AC

2 value. We operated the calibration loop with different artificial gas cylinders of known CO and

3 CH4 mixing ratios. Reference and CO mixing ratios of these cylinders are reported in Table S3.

4 Gas flow injected through the calibration loop was later adjusted if required so as the calibration

5 loop reproduces nicely the expected methane preferential dissolution. We note that such

6 adjustments were more pronounced at IGE than at DRI, showing that the geometry of the

7 calibration loop itself can also impact how gas dissolves within the CFA setup.

8 After and/or before each calibration loop experiment, gas from all cylinders (Table S3) were

9 analysed directly with the OF-CEAS analyser. We know that the internal calibration of the SARA

10 analyser is very stable with drift over periods of time of few hours. The Calibration Loop data were

11 not calibrated onto the NOAA/WMO X2014 scale, but instead directly compared to these "dry"

12 measurements.

13 **1.8.3. Calibration parameters**

14 Each continuous CO dataset, after initial calibration of the OF-CEAS analyser (Sect. 1.2), was

15 calibrated using multi-standards calibration loop dataset. As an example, Fig S4 reports the multi-

16 standards calibration loop dataset obtained for the 2013 DRI analytical campaign (with two

17 degasser configurations). The following can be extracted from such calibration datasets:

18 $[CO]_{COR} = ([CO]_{SAMPLE} - CO_{BLANK}) / SC$

19 With CO_{BLANK}, the CO blank of the CFA setup determined for each analytical campaign (Sect. SI

20 1.5), and SC the Solubility Correction evaluated with CL experiment (Sect SI 1.8.2). Table S2

21 reports SC (and CO blank) for each ice core analysed. The lowest SC, i.e. 3.7%, was observed

22 during the DRI 2013 campaign, when using a Membrana Micromodule degasser. The SC

23 observed when using an Idex Transfer-Line degasser ranged [6.0-8.8]%; this limited SC range

24 includes 3 different CFA configurations (DRI 2013, DRI 2015, and IGE 2017).

25 **1.8.4. Evaluating Internal CFA calibration**

26 CO has a low solubility, and SC observed were always below 10%. However, our internal CO

27 CFA calibration had to be evaluated. To do so, five 986 g discrete samples from the PLACE core

28 were analysed at UR, following a modified version of the protocol detailed on Sect. SI 1.10 in

29 which the ice samples are not grated into a powder and standard gas is not added to the vessel

30 before melting the sample. [CO] obtained from these discrete measurements can be compared

31 to the continuous CFA dataset, collected at both DRI (2015) and IGE (2017). Only five samples

1   were analysed discreetly, as this analytical capability was designed only in late 2019, and applied

2   in priority to investigate if high frequency CO spikes observed in Greenland continuous CO

3   records could be driven by in-extractu, production as described in Sect. 3.2.4 (in-extractu CO

4   production occurs during the melting analytical process). However, the depths of the five discrete

5   samples described here ranged the entire core, from 84 to 146 m depth. Blank corrections were

6   applied by subtracting the average of four gas free ice runs (CO mole fraction = 9.0 ± 2.1 ppbv)

7   that were run concurrently with the five PLACE core samples. The CO mole fraction measurement

8   uncertainty for the five PLACE cores samples was defined as the CO mole fraction variability

9   of the gas free ice measurements.

10   A direct comparison of discrete and continuous dataset is reported on Fig. S7. The standard

11   deviation of the differences between discrete and CFA-based CO measurements is 1.8 ppbv and

12   2.8 ppbv for the IGE (n=5) and DRI (n=4), respectively. The average offset between discrete and

13   CFA-based CO measurements is 1.3 ppbv and 2.1 ppbv for the IGE (n=5) and DRI (n=4),

14   respectively. This excellent agreement supports our approach to internally calibrate continuous

15   CO, and demonstrates that continuous [CO] dataset can now be accurate, which is an important

16   improvement since the NEEM-2011-S1 measurements (Faïn et al., 2014).

Faïn et al., 2021, CP, Supplementary Information
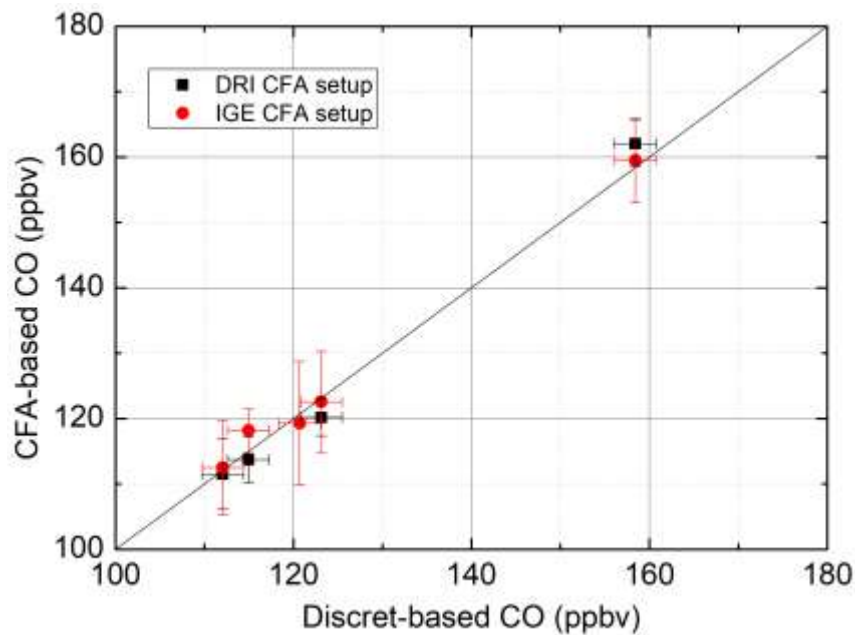
1 **Figure S7.** Comparison of CO mixing ratios measured on the PLACE ice core by discrete or continuous

2 methods. Continous [CO] values are calculated as the mean CFA [CO] levels on the depth intervals

3 spanned by discrete samples. Discrete dataset is compared with both DRI and IGE continuous CO dataset.

4 Sample depth intervals encompassed the entire span of the PLACE core, from 84 to 146 m depth.

5 **1.9. Smoothing of continuous CO measurements**

6 1.9.1. Impulse responses of CFA systems

7 Due to mixing and dead volumes, the CFA system introduces a smoothing of the gas signals.

8 Using the method described in Stowasser et al. (2012), we measured during each analytical

9 campaign the switch between two mixes of deionized water and standard gases (Fig. S8-11, left

10 panels). It allowed us to determine step responses of the CFA systems, which is not instantaneous

11 but spreads over time. During the 2013 DRI campaign, both Idex Transfer-Line and Membrana

12 Micromodule degassers were used (Table S2), and step responses were determined for each

13 degasser configuration.
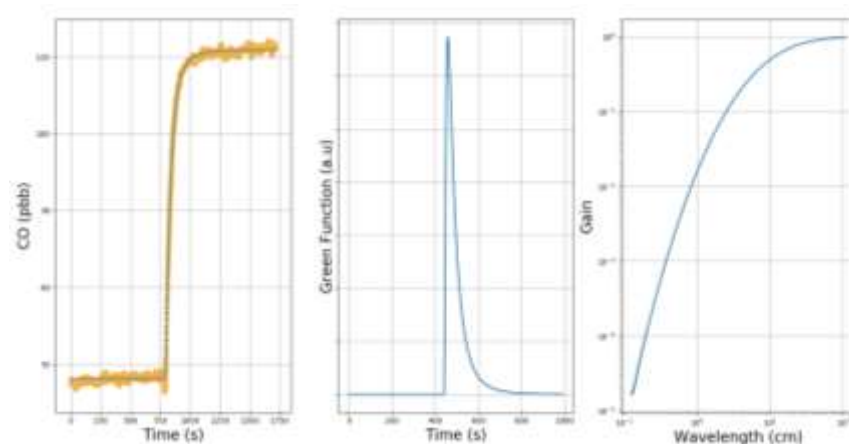
15 **Figure S8.** Left panel: step response of the DRI CFA system operated with a Micromodule (Membrana)

16 degasser in 2013 for analyzing the Tunu13, D4, and NEEM-SC ice cores. Orange dots: measurement

17 points. In blue: fit by the cumulative density function of a log-normal law. Middle panel: Green's Function of

18 the CFA system approximated by a log normal law. Right panel: Gain of the CFA system against the

19 wavelength of sine signals. Gray lines correspond to the cut-off wavelength and a 50% attenuation
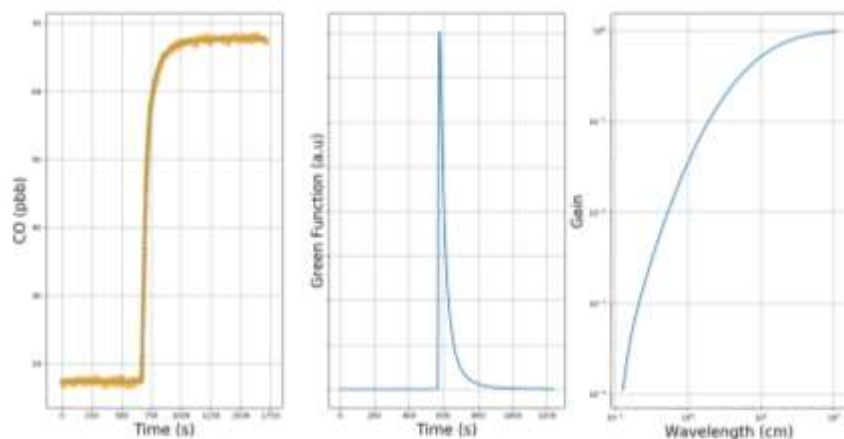
2 **Figure S9.** Same as Figure S8 for the DRI CFA system operated with a Transfer Line (Idex) degasser in

3 2013 for analyzing the NEEM-SC and the NGRIP ice cores.
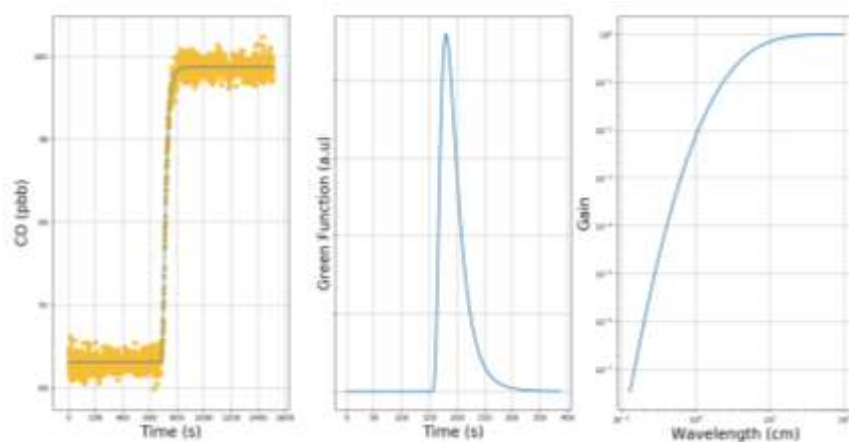
6 **Figure S10.** Same as Figure S8 for the DRI CFA system operated with a Transfer Line (Idex) degasser in

7 2015 for analyzing the PLACE ice core.

Faïn et al., 2021, CP, Supplementary Information
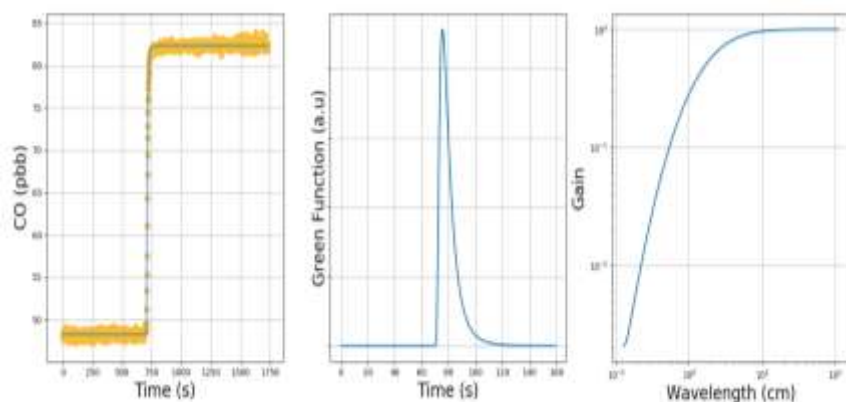
2 **Figure S11.** Same as Figure S8 for the IGE CFA system operated with a Transfer Line (Idex) degasser in

3 2017 for analyzing the PLACE ice core.

5 Each observed step response was fitted using the cumulative density function of a log-normal

6 distribution. These log-normal distributions (Fig. S8-11, middle panels) can be considered as the

7 Green's functions, or impulse responses of the CFA systems. Finally, the Green's functions can

8 be used to derive the frequency responses of the systems using Fourier transforms, that is to say

9 the attenuation factors (also referred to as gains) experienced by a sine signal depending on its

10 frequency/period/wavelength. A cut-off wavelength can be defined as the wavelength of a sine

11 signal experiencing a 50% attenuation in amplitude. It is important to note that this cut-off is

12 defined for sine signals, and therefore cannot be directly applied to other types of signals. For

13 instance, Fourteau et al. (2017) reports that a square signal will be less attenuated than a sine

14 signal.

15 During the 2013 DRI campaign, we observed with a melting rate of 5.5 cm min^{-1} cut-off

16 wavelengths of 15.0 cm and 14.2 cm, when using a Micromodule or a Transfer-Line degasser,

17 respectively. A Micromodule was used for the D4, Tunu13, part of NEEM-SC, cores, and a

18 Transfer-Line degasser was used for NGRIP, and a fraction of NEEM-SC (Table S2). During the

19 2015 DRI campaign, we used an Idex Transfer-Line degasser optimized, i.e. shortened to reduce

20 its internal volume to only 1 mL. Consequently, we observed with a melting rate of 5.5 cm min^{-1}

21 a cut-off wavelengths of 9.3 cm. During the 2017 IGE campaign, we used the same shortened

22 Transfer-Line degasser, but the entire gas setup was optimized specifically for gas measurements

23 (including the use of a low dead volume glass debubbler): a cut-off wavelength of 1.6 cm was

1 observed. Similar improvements were investigated on the DRI CFA setup in 2015, but could not
2 be fully implemented because they would have decreased the resolution of the liquid phase
3 analyses conducted simultaneously to CO continuous measurements.

1.9.2. Modeling the impact of CFA analytical smoothing on CO baseline for the Tunu13
core

7 The Tunu13 ice core was analysed with the 2013 DRI CFA setup (Micromodule degasser), which
8 exhibit the largest response time in the gas phase (Table S2, Fig. S8). This effect is compounded
9 by the low snow accumulation rate of Tunu13. Step tests (Sect. SI 1.9.1) suggest that for CO a
10 60% attenuation would be expected for a sine signal of 10 cm wavelength, a depth interval
11 representing >1 yr.

12 To further investigate how analytical smoothing can alter the CO 5th baseline levels of the Tunu13
13 archive, the following modeling was conducted:

14 - A synthetic signal representing the original Tunu13 CO signal is produced as follow: the
15   baseline is set to a constant 80 ppbv value, with abrupt CO spikes superimposed. These
16   spikes are limited to summer layers (lasting 2 months), and their amplitudes are distributed
17   using a normal law. Smoothed amplitudes of the synthetic CO spikes are similar to the [CO]
18   spike levels observed in the Tunu13 dataset collected at DRI in 2013 (Fig. 1). This original
19   (i.e., before smoothing) synthetic signal is reported in orange in Fig. S12.
20 - The synthetic signal is convoluted with the DRI-2013 CFA setup Green function, and a
21   smoothed signal is thus observed (reported in blue in Fig. S12)
22 - A 5th percentile baseline is extracted from the smoothed signal, and compared to the original
23   baseline, i.e. the constant 80 ppb levels.

Faïn et al., 2021, CP, Supplementary Information
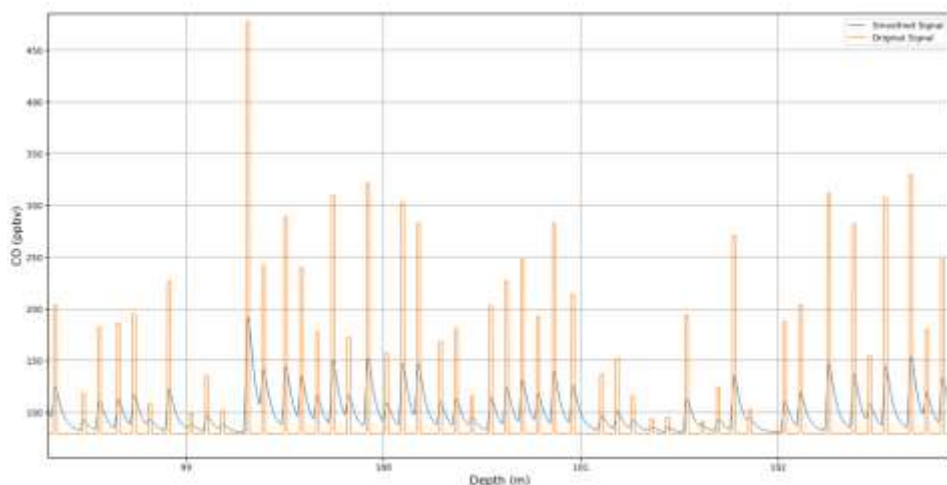
2 **Figure S12.** A synthetic CO signal where abrupt CO spikes are superimposed on a 80 ppbv constant

3 baseline (orange). Spikes are repeated annually, using an accumulation rate of 8 cm weq yr-1 (i.e., lowest

4 value observed along the Tunu13 record) and their duration is set to 2 months; spike amplitudes are

5 distributed according to a normal law. In blue we report the convolution of the synthetic CO record with the

6 analytical green function of the 2013 DRI CFA system.

8 Figure S13 reports the increase in baseline due to CFA analytical smoothing (DRI 2013 setup),

9 for a synthetic signal representative of the low-accumulation (i.e., 8 cm weq yr-1) section of the

10 Tunu13 core. Although the increase averaged over the entire 40 m long record is limited (3.7 ±

11 1.7 ppbv), it reaches locally 8 ppbv for depth intervals spanning few meters.

Faïn et al., 2021, CP, Supplementary Information
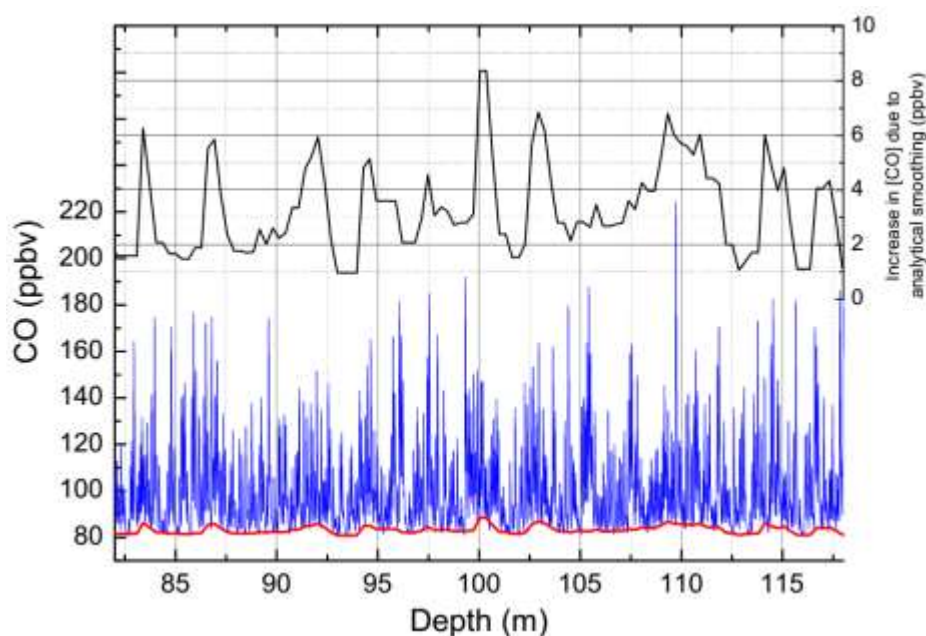
2 **Figure S13.** Increase in CO baseline due to analytical smoothing (DRI 2013, Micro-module setup) for a

3 synthetic signal exhibiting a Tunu13 accumulation rate of 8 cm weq yr-1 (black line). The smoothed

4 synthetic signal (blue line) and the 5th percentile baseline extracted for that signal (red line) are reported on

5 the same depth scale.

7 Similar approach was applied to simulate analytical smoothing affecting other records discussed

8 in this study. It shows the baseline's enhancement due to analytical smoothing and impacting

9 other record was limited to a local maximum of 2 ppbv.

11 **1.10. Impact of storage on CO mixing ratios**

12 A 10 m long replicate section of the PLACE core was analyzed nearly two years after the main

13 analytical campaign (respectively December 2018 and February 2017) and no change in the CO

14 values was observed (Fig S14), supporting that CO production in ice during core storage is

15 unlikely.

Faïn et al., 2021, CP, Supplementary Information
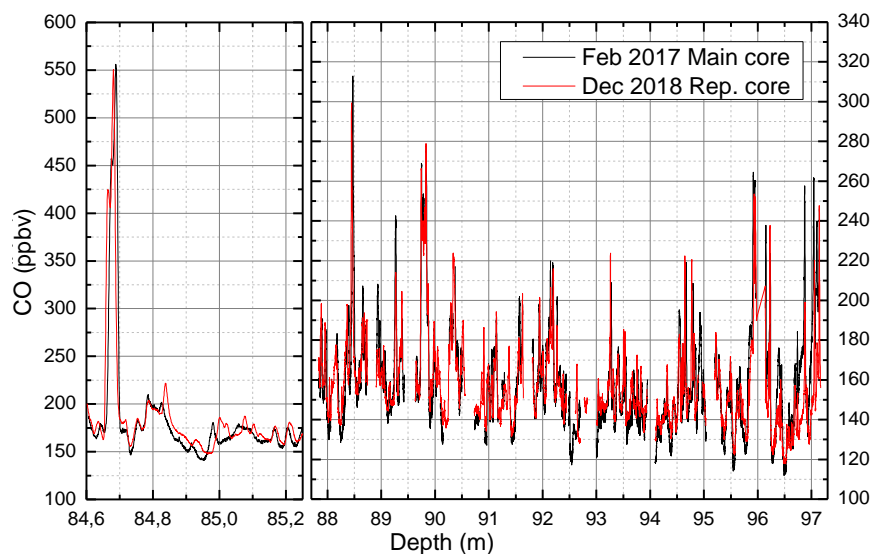
Figure S14. Replicate measurements of CO mixing ratios (Main cuts in black, Replicate cuts in red) conducted on the PLACE core at IGE: replicate sections were analyzed 20 months after the main CFA campaign (in Dec. 2018 and Feb. 2017, respectively).

1.11. Discrete CO analyses

[CO] analyses on discrete ice and firn core samples (including the PLACE core) were carried out at the University of Rochester (UR), with the goals of investigating the possibility of "in-extractu" production of CO during melting of ice core samples from trace organics contained in the ice, as well as to verify that there were no additional uncharacterized artifacts associated with the continuous [CO] method.

1.11.1. Ice Handling and Melting

Ice and firn samples are prepared by first removing 0.5 cm of ice from all sides of the sample with a bandsaw using a precleaned blade and solid ceramic bearings. The samples are further cleaned using a stainless steel cheese grater to remove an additional 1-3 mm from all sides. The cleaned samples are placed into a prechilled (-20°C) glass extraction vessel and held in a clean air box flushed with CO-free air. The solid ice (non-firn) samples were grated further to destroy the ice

1   matrix and remove the trapped air. The resulting powder is collected into the extraction vessel.

2   These sample tests are referred to as "Powder Tests".

3   The melting vessel is attached to the air extraction line via a PTFE O-ring that has been

4   continuously flushed with CO-free air to ensure the O-ring will not outgas CO. The extraction

5   vessel is then evacuated, and the integrity of the O-ring seal is verified. A cold bath (-15°C) is

6   applied to the extraction vessel to keep the sample cold and a flow of CO-free air (50sccm) is

7   started to flush the ice sample for at least 12 hours before the sample is run. In addition, a flow of

8   CO-free air (150 sccm) is also flushed around the exterior PTFE O-ring seal to ensure the O-ring

9   does not allow any room CO to diffuse into the extraction vessel during flushing and the

10   extractions.

11   After flushing, the vessel is again evacuated for at least 30 minutes before a known amount of

12   CO standard gas is introduced; the vessel is then isolated from the rest of the system. The sample

13   is melted over ~50 min using a warm water bath maintained at 50°C. The warm water bath is

14   removed while a small amount of ice is still left in the extraction vessel and an ice bath is applied

15   for a minimum of 10 minutes before starting measurements; the ice bath is left on the vessel

16   during the rest of the process.

17   **1.11.2. CO Concentration Measurements**

18   The gases in the headspace of the extraction vessel (sample gas) are measured for CO

19   concentration at regular intervals using a reducing gas detector (RGD; Peak Performer 1 from

20   Peak Laboratories). A small aliquot of sample air is expanded into a section of the Pyrex extraction

21   line known as the "Large Volume Loop" (LVL; volume of 155 scc) and the expansion pressure is

22   measured. Ultra-High Purity Air (UHP Air) is then admitted into the extraction line at a steady, low

23   flow rate (50 sccm) to ensure laminar flow in the system. This UHP Air serves as a "push" gas,

24   compressing the sample aliquot into the sample loop of the RGD (the RGD is intended for

25   operation with ambient-pressure samples). A simplified schematic of the UR analytical setup

26   dedicated to discrete CO measurements is reported on Fig. S15.
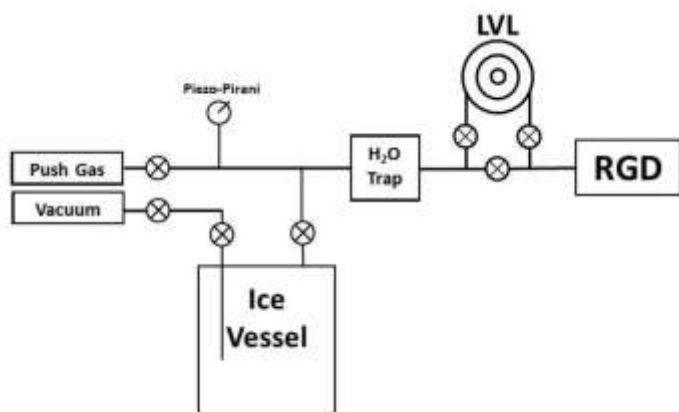
2   **Figure S15.** A simplified schematic of the expansion volume used for the discrete CO measurements.

3   Sample gas is held in the Ice Vessel and expanded into the "LVL" (Large Volume Loop, ~155 cm^3 volume)

4   and into the "RGD" for measurement. Water vapor is removed by the H_2O trap held at ~-60°C with a dry

5   ice and ethanol mixture and the line pressure is monitored with the Piezo-Pirani pressure gauge. The

6   expanded gas is then compressed via a flow of a "push" gas at 50 sccm to ensure laminar flow and prevent

7   rapid mixing with the sample gas. The sample loop in the "RGD" (1 cm^3 volume) is pressurized to 1013

8   mbar for measurement. The sample CO mole fraction is measured by the '"RGD" which is a Peak Performer

9   1 (Model PP1 from Peak Laboratories) Reducing Gas Detector.

11 Once the RGD sample loop is pressurized to 760 torr, the sample aliquot is injected and analysed

12 for CO concentration. Between each expansion of sample gas from the extraction vessel, a CO

13 standard is directly measured. This is accomplished by filling the RGD sample loop with a CO

14 standard gas to ambient pressure. The first 20 scc of standard gas is discarded by flushing to

15 either atmosphere or vacuum, after which the standard gas is pressurized (again to 760 torr) and

16 injected. These standard gas measurements allow for the CO concentration of the sample gas to

17 be calculated and for instrumental drift to be corrected for during the tests.

18 Sample gas aliquots are expanded from the vessel several times during the run, to observe the

19 growth of excess CO. All tests are run in a similar manner with similar timings. The first expansion

20 of sample gas from the vessel (Expansion 0) is performed immediately after the standard gas is

21 added to the vessel and before melting is started. This expansion is a baseline check of the

22 system to ensure no major issues are present before the test is run in full.

1 Following this, melting is started and a second expansion (Expansion 1) is performed when

2 around 0.5cm of water is present in the bottom of the vessel. This expansion occurred about 35

3 minutes after Expansion 0, with the next expansion (Expansion 2) occurring about 20 minutes

4 later, just before melting finishes, at about the time the ice bath is applied to the vessel. The last

5 three expansions (Expansions 3-5) take place about 30, 60 and 120 min after melting is complete.

6 Expansions 0-5 are reported along a time scale on Fig.3 of the manuscript.

7 **1.11.3. Types of Tests and Data Corrections**

8 To account for the procedural CO blank of the extraction line, two types of tests were performed.

9 The first is the "No-Melt" test, where the procedure is as described above except that the ice

10 sample is not melted but kept at -15°C the entire time. The average blank from all No-Melt

11 extractions was 3.2±1.7 ppbv. The second run type is the "Melt" test, involving the full procedure

12 (including melting) described above. In many cases (Table S4), the No-Melt test was performed

13 immediately prior to a Melt test on the same sample. The No-Melt test [CO] values were

14 subtracted from the Melt test [CO] values to isolate the effect of the melting step on [CO]. When

15 a No-Melt test was not available for a given sample, the average of No-Melt tests run in a similar

16 fashion to the Melt test was used to subtract the extraction line [CO] blank.

17 The rate at which sample aliquots were expanded out of the vessel ("slow expansion" or "fast

18 expansion"; Table S4) was reduced approximately in the middle of this set of tests, as it was

19 determined that faster expansion may have allowed some water vapor to break through the

20 cryogenic trap, potentially causing an elevated response in the RGD detector (higher [CO]). The

21 results of the tests conducted using fast expansions were further corrected for this effect (1.9

22 ppbv), based on a comparison of tests run on depth-replicate firn samples using fast versus slow

23 expansions.

24 The amount of excess CO produced from melting was calculated by subtracting the starting CO

25 concentration before melting (expansion 0) from the final CO concentration after melting

26 (averaging expansions 2-5). When the starting value (expansion 0) was not available (n=2), an

27 average of starting values (expansion 0) from similar runs was used instead. This "excess CO"

28 represents our best estimate of CO increase that is attributable solely to the melting step.

29 Finally, replicate firn samples run in "solid" and "powder" modes showed similar results (Table

30 S4), allowing to ensure that the extra sample processing (grating step) needed for ice samples

31 did not result in excess and variable CO production in the ice samples.

Faïn et al., 2021, CP, Supplementary Information

Sample Reference	Top Depth (m)	Bottom Depth (m)	Powder Test?	Melt Time (Minutes)	Sample Size (kg)	Standard Gas added (cc STP)	TOC (ppbC)	Continuous [CO] (ppbv)	Excess CO, discrete analyses (ppbv)
Gas Free Ice	-	-	Yes	30	0.743	226.2	≤ 2.0	n.d.	9.3
Central Greenland Firn 1-A	45.10	45.30	No	78	1.089	191.4	n.d.	n.d.	7.6
Central Greenland Firn 1-B	45.10	45.30	No	76	0.92	191.9	n.d.	n.d.	9.9
Central Greenland Firn 1-C	45.10	45.30	No	42	0.813	200.0	n.d.	n.d.	7.5
Central Greenland Firn1- D	45.10	45.30	No	48	1.015	197.4	n.d.	n.d.	6.1
Central Greenland Firn 2-A	44.89	45.06	No	61	0.935	209.4	n.d.	n.d.	5.8
Central Greenland Firn 2-B	44.89	45.06	No	45	0.819	222.6	n.d.	n.d.	3.7
Central Greenland Firn 2-C	44.89	45.06	Yes	43.5	0.66	237.6	n.d.	n.d.	7.8
Central Greenland Firn 2-D	44.89	45.06	Yes	39	0.788	222.0	n.d.	n.d.	5.8
Central Greenland Firn 3-A	44.72	44.89	No	44	0.809	219.9	n.d.	n.d.	5.9
Central Greenland Firn 3-B	44.72	44.89	Yes	33	0.678	232.0	n.d.	n.d.	2.4
Central Greenland Firn 3-Small-A	44.72	44.80	No	33	0.379	189.5	n.d.	n.d.	5.4
Central Greenland Firn 3-Small-B	44.63	44.71	No	28.5	0.272	192.5	n.d.	n.d.	4.7
Central Greenland Firn 3-Small-C	44.72	44.80	No	34.5	0.298	198.1	n.d.	n.d.	4.2
Central Greenland Firn 3-Small-D	44.63	44.71	No	27	0.3	196.1	n.d.	n.d.	4.7
PLACE ice: elevated CFA [CO]-A	110.69	110.48	Yes	30	0.793	197.8	26.0	186.3 ± 27.7	7.2
PLACE ice: elevated CFA [CO]-B	110.69	110.48	Yes	48	0.682	212.7	26.0	186.3 ± 27.7	6.6
PLACE ice: low CFA [CO]-A	109.76	109.69	Yes	26	0.604	201.3	18.4	128.7 ± 10.6	3.6
PLACE ice: low CFA [CO]-B	109.69	109.52	Yes	43	0.661	212.4	16.0	129.7 ± 8.0	4.3
Taylor Glacier (Antarctica, 15 kyrs old)	≈6	-	Yes	41	0.626	237.8	n.d.	n.d.	6.2
Taylor Glacier (Antarctica, 6 kyrs old)	≈6	-	Yes	28.5	0.674	210.6	n.d.	n.d.	8.3

Table S4. Sample information for tests used to investigate the hypothesis of rapid CO production from trace organics in the ice during ice melting. Firn samples were all taken from a firn core from Summit, Central Greenland (camp C14), and are denoted by a number and letter combination; the number is the depth level (1-3) and the letters are the replicate sample (A-D) from that level. The "Small" Firn samples came from Firn block 3-C and Firn block 3-D, which were cut in half to create "Small" Firn samples A-D. PLACE ice samples follow a similar naming scheme, with the number representing the depth level and the letter indicating the replicate sample. The "PLACE ice: low CFA [CO]" samples were selected from two distinct sections of the PLACE core that displayed a minimal amount of the high frequency variation in the CFA CO record, with no large CO peaks observed, whereas the "PLACE ice: elevated CFA [CO]" samples were taken from a region with a large amount of the high frequency variation in the CFA CO record and large CO peaks observed. Sample ice from Taylor Glacier (Antarctica) was used and is labeled by age of the ice as only a single sample of each was run. Lastly, "Gas Free Ice" was produced in the laboratory and used as a control sample. The "Excess CO" reported in the table is the average of Expansion 2-5 for a given sample and has been blank corrected.

Faïn et al., 2021, CP, Supplementary Information

2. Continuous CO dataset

2.1. Revisiting NEEM-2011-S1 CO data calibration

For the first time, continuous [CO] was collected along the NEEM-2011-S1 core at DRI, in 2011 (Faïn et al., 2014), by coupling a continuous melting setup with a laser (OF-CEAS) spectrometer. While this analytical setup generated stable measurements of CO concentrations with an external precision of 7.8 ppbv (1σ), it suffered from a poor accuracy. Absolute calibration of the NEEM-2011-S1 dataset could not be established by Faïn et al. (2014).

In the framework of this study, we had the opportunity to analyze samples from the NEEM-SC core. These NEEM-SC samples showed a 10 m overlap in depth with the NEEM-2011-S1 record (overlap spanning 399–409 m depth), and then extended deeper. It was of high interest to reevaluate the CFA-based calibration of the NEEM-2011-S1 core so as to obtain a coherent NEEM composite record.

During the NEEM-2011-S1 campaign, for the first time we attempted to use a calibration loop to evaluate (i) blank, and (ii) solubility of continuous CO data. However, the CL did not work properly, resulting in a highly uncertain CO blank (48±25 ppbv), and no internal calibration. Here, we reprocessed the NEEM-2011-S1 CO data using the CO blank and internal calibration established for the NEEM-SC core analyzed 2013 (35±7 ppbv, and 0.96 solubility correction). A fraction of the NEEM-SC core (depth intervals: 573–491m and 444–399 m) was indeed analyzed with a CFA system similar to the one set up in 2011 for the NEEM-2011-S1 core.

Figure S16 shows the good agreement when NEEM-2011-S1 reprocessed data and the NEEM-SC data overlap over the 399-409 m interval. Such good agreement did not exist when using the NEEM-2011-S1 data as initially processed by Faïn et al. (2014).

Faïn et al., 2021, CP, Supplementary Information
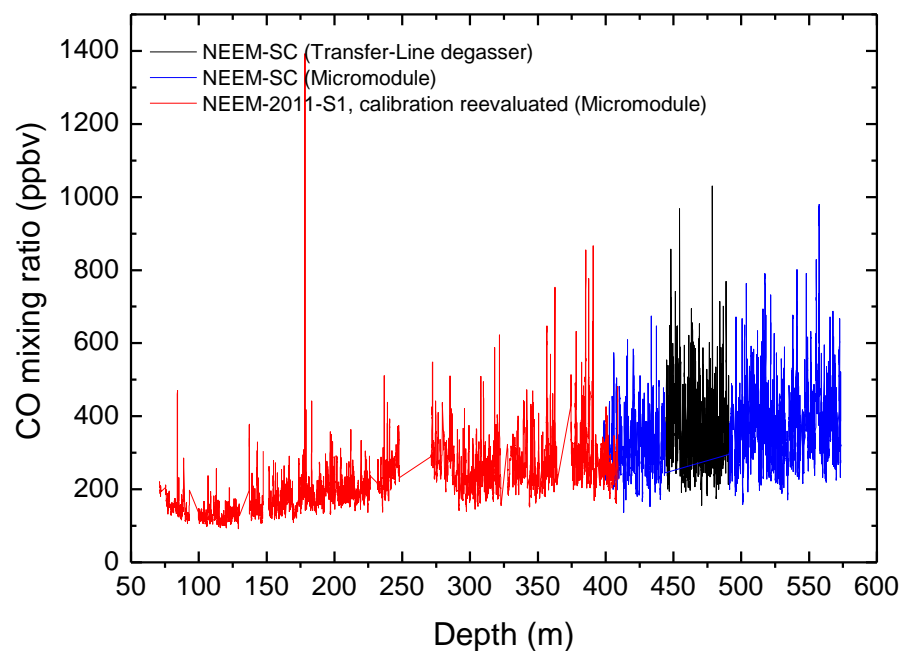
Figure S16. Continuous CO dataset measured on two different cores collected at the NEEM site: the
NEEM-2011-S1 core, and the NEEM deep core (SC archive section). NEEM-2011-S1 and NEEM-SC
dataset overlap over the 399-409 m interval. The NEEM-2011-S1 core calibration has been revised in the
frame of this study. The NEEM-2011-S1 was analyzed with a Micromodule degasser. The NEEM-SC core
was analyzed with either a Transfer-Line or a Micromodule degasser.

2.2. Full Continuous CO records

Figure S17 reports the full continuous [CO] records measured along the ice cores investigated in
this study: Tunu13, D4, NEEM (SC and 2011-S1 combined), PLACE (DRI) and NGRIP.

Faïn et al., 2021, CP, Supplementary Information
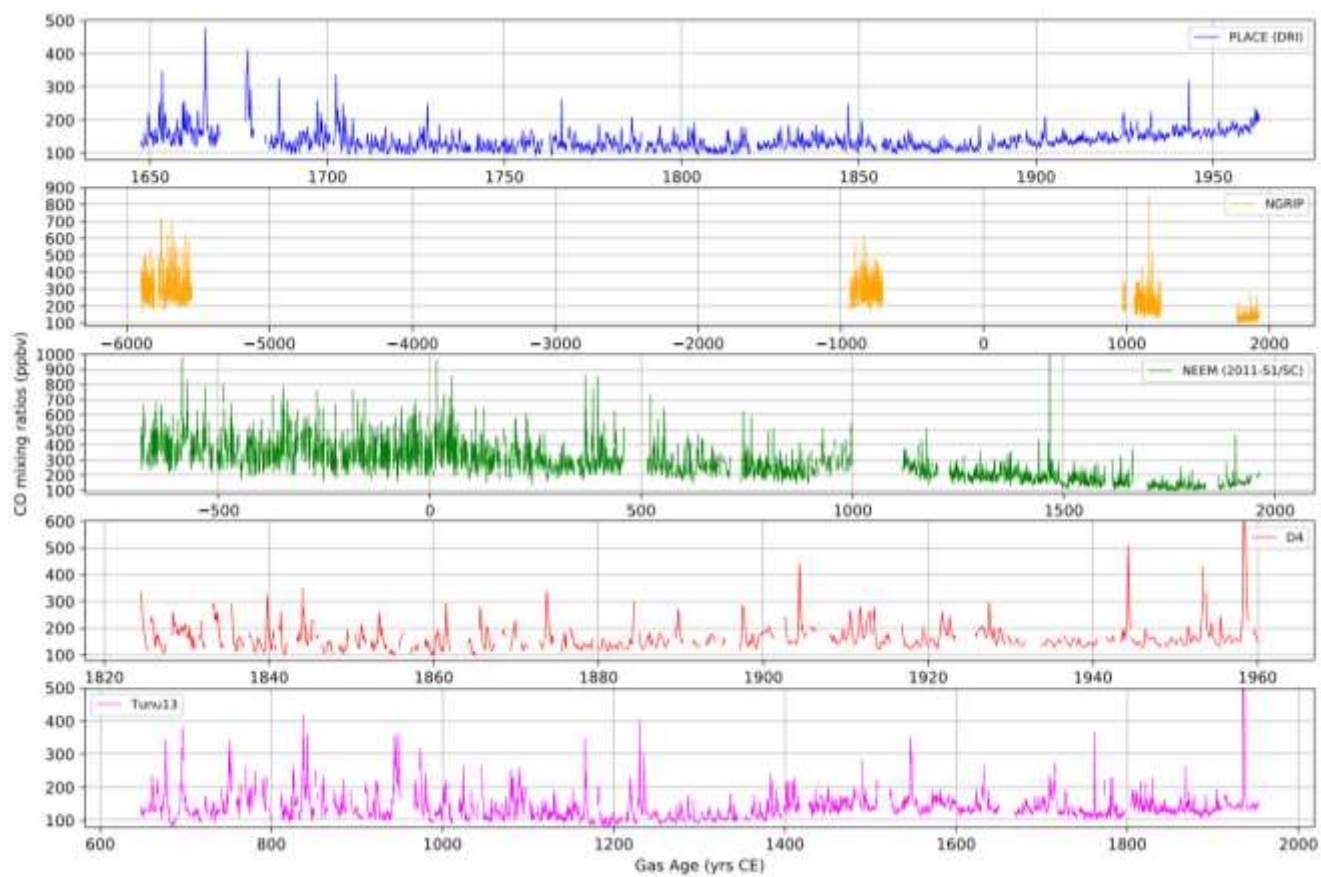
2 **Figure S17.** Full continuous [CO] dataset for the Place (DRI), NGRIP, NEEM (combining NEEM-2011-S1 and NEEM-SC cores), D4, and Tunu13

3 ice cores.

Faïn et al., 2021, CP, Supplementary Information

1 **2.3. Median Absolute Deviation**

2 Figure S18 reports the MAD (Median Absolute Deviation) for the CO records investigated in this
3 study.
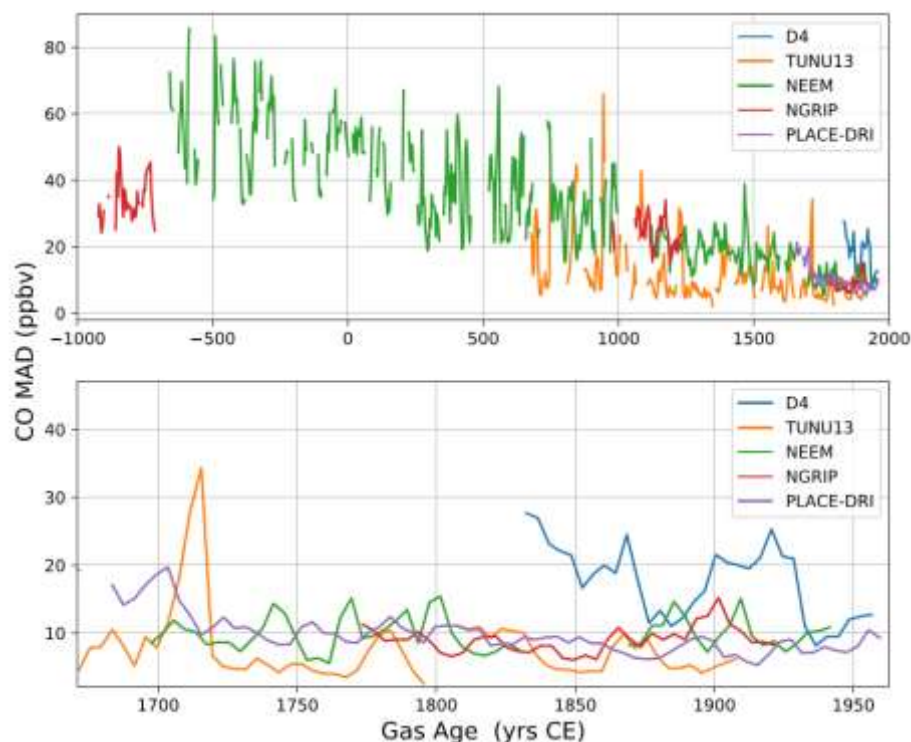
5 **Figure S18.** CO Median Absolute Deviation (MAD) for the Place (DRI), NGRIP, NEEM (combining NEEM-
6 2011-S1 and NEEM-SC cores), D4, and Tunu13 datasets.

8 **2.4. Comparing DRI and IGE PLACE continuous CO records**

9 In the framework of this study, the PLACE core was analysed for continuous, high resolution, CO
10 mixing ratio with both the DRI (USA) and IGE (France) CFA setups (Table S2). The PLACE core
11 was drilled in June 2015, and analysed at DRI in September 2015. The CFA-based CO
12 measurements were conducted at IGE 18 months later, in February 2017. The PLACE core was

1 stored at <-20°C at NICL prior to being shipped to France. During the shipment, the ice remained

2 at <-20°C.

3 Figure S19 reports both DRI and IGE continuous CO datasets. The two records are extremely

4 similar in the 115-153 m depth interval. However, DRI and IGE CO records exhibit differences in

5 the 80-115 m depth interval: while CO spikes are located at the same depths in the IGE and DRI

6 records (e.g., Fig.2 of the manuscript), their amplitudes are larger in the IGE record.
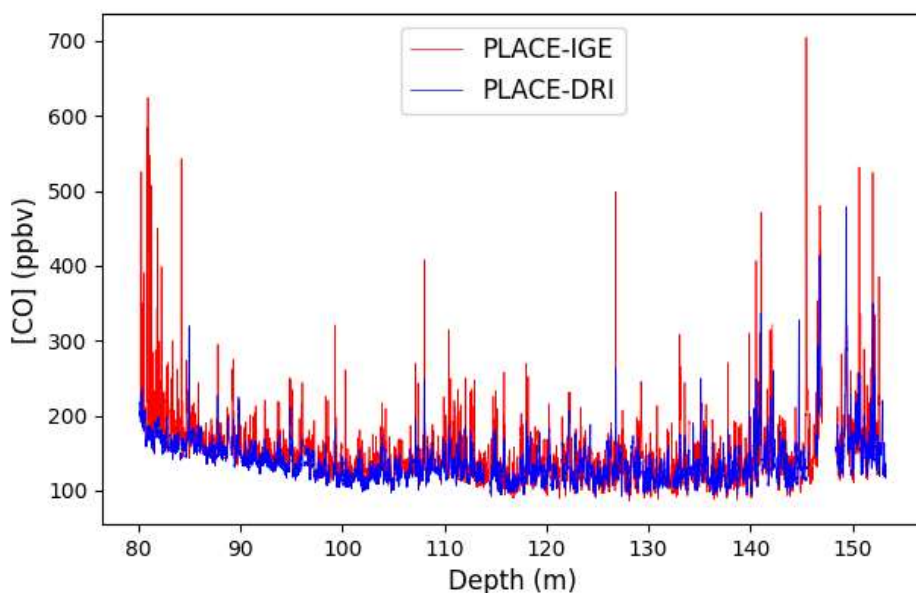
8 **Figure S19.** PLACE continuous CO records collected on the DRI and IGE CFA setups in September 2015

9 and February 2017, respectively.

11 Figure S20 compares mean and 5th percentile (i.e., baseline) CO extracted from the DRI and IGE

12 high resolution datasets. Mean and 5th percentile of the data are calculated every 4 years over a

13 moving window of 15 yrs. Shaded envelopes reported in Fig. S20 represent the uncertainties (1σ).

14 The PLACE CO baseline extracted from the IGE continuous record is similar to the one based on

15 the DRI dataset: both baselines agree within their uncertainty envelopes. Replicate datasets (Fig.

16 S3) further rule out analytical drifts of the DRI or IGE CO baselines during the measurements: in

17 both laboratories, we first melted the entire core, and later some replicate sections were

1   reanalyzed. Such replicate measurements exhibit an excellent agreement with the main records
2   (Fig. S3).
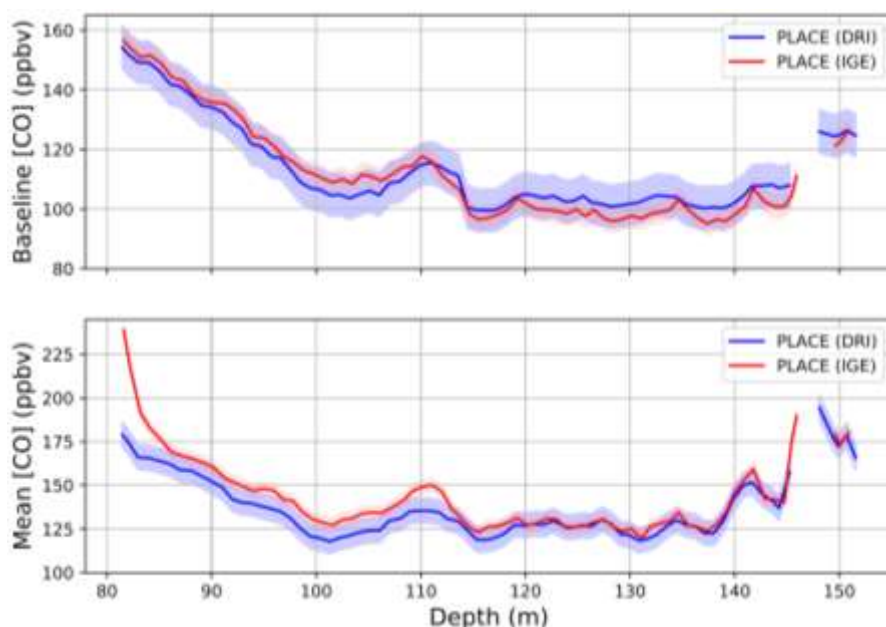
4   **Figure S20.** Comparison of means and 5th percentiles (i.e., baseline) CO signals extracted from the
5   continuous CO records measured on the DRI and IGE CFA setups. Shaded envelopes represent the
6   uncertainties.

8   The PLACE mean CO mixing ratios measured at DRI and IGE are in excellent agreement along
9   the 115-153 m depth interval (Fig. S17). However, mean CO mixing ratios measured at IGE are
10 ~10 ppbv higher than the DRI levels in the 85-115 m depth range, and much higher in the 80-85
11 m depth interval. Comparison of high resolution, continuous, methane datasets collected
12 simultaneously to CO with both the IGE and DRI CFA setups reveal elevated and abrupt [CH4]
13 patterns exiting only on the IGE record (Fig. S21) in the 80-85 m depth interval. We thus
14 hypothesize that post-coring entrapment of modern air (e.g., Aydin et al., 2012) during the 18
15 months storage prior to the IGE analytical campaign can explain [CO] enhancement observed on
16 the IGE record.
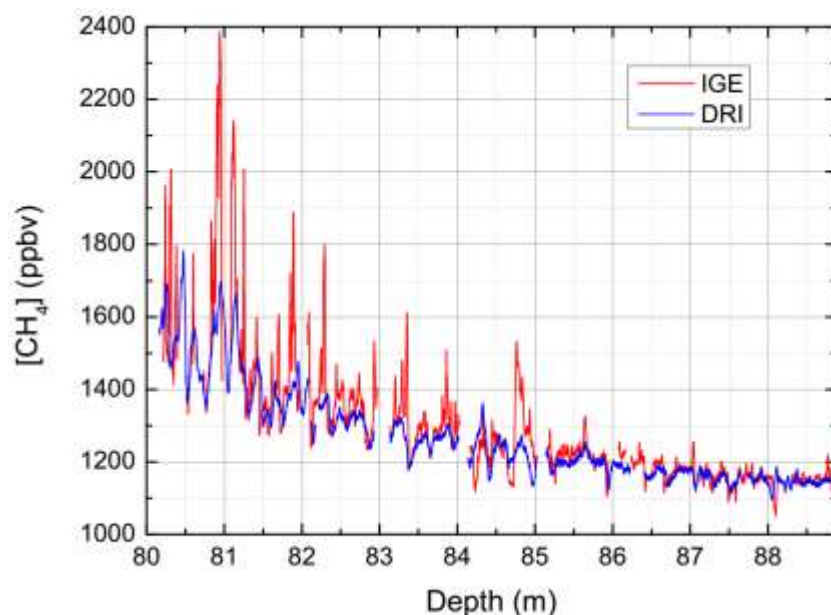
Figure S21. High resolution methane measurements collected simultaneously to CO with the DRI (resp.
IGE) CFA setup, and reported in blue (resp. In red). The elevated and spiky methane pattern observed on
the IGE dataset reveals contamination of the gas IGE CFA by modern air on the 80-85 m depth interval.

The reason for why the 85-115 m depth interval of the IGE CO record exhibits higher mean and
CO spikes (but similar CO baseline) remains unexplained. We do not expect that the 18 months
storage period between DRI and IGE PLACE analytical campaigns would impact CO patterns, as
indicated by replicate measurements made 22 months apart (Fig. S14). Laboratory investigations
conducted on discrete samples support the idea that the elevated and highly variable [CO] values
observed in Greenland ice samples are due to excess CO produced from in situ production within
the ice itself rather than extraneous CO production during ice melting (Sect. 3.2.4), and this
conclusion should apply to both DRI and IGE CFA setups. Further, offsets between the IGE and
DRI records caused by procedural artifacts would be expected to affect the entire record, not just
the parts of the cores shallower than 115 m.

Overall, the difference between continuous CO records collected at DRI and IGE remains small,
with a gap in mean levels never exceeding 10 ppbv for ice sections which are not near the firn-
ice transition, and this offset does not affect our conclusions regarding baseline CO trends.

2.5. Seasonal distributions of CO mixing ratios for the PLACE record
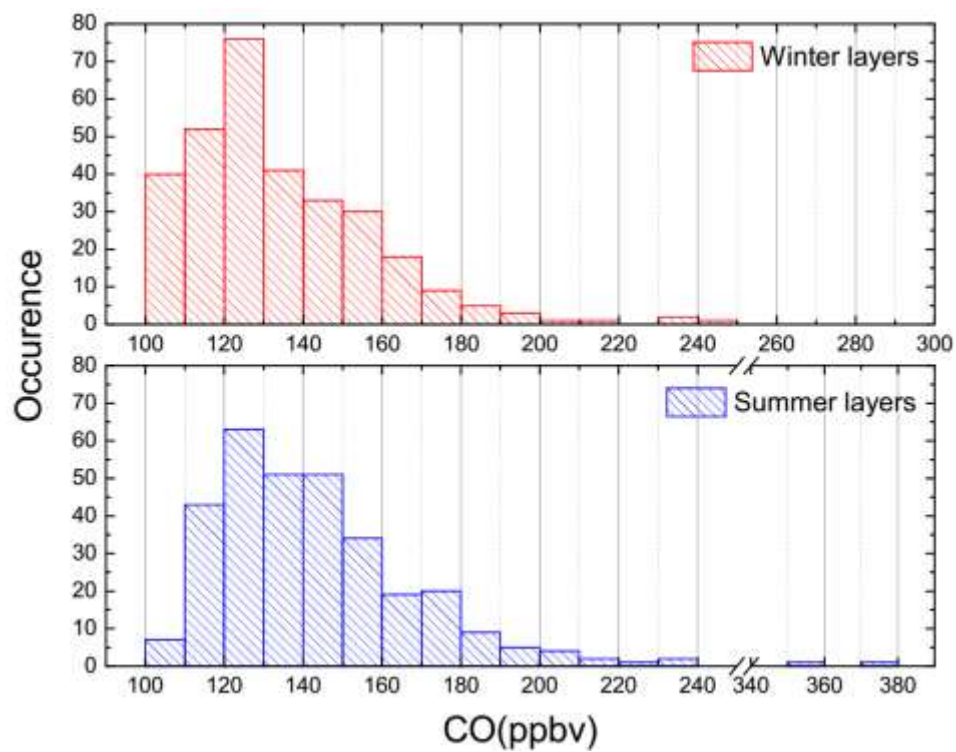
Figure S22. Seasonal distributions of CO mixing ratios for the full PLACE record. Summer (resp. winter)
refers to the 6 months period spanning April-September (resp. October-March).

Faïn et al., 2021, CP, Supplementary Information

1   **2.6. Comparison of Eurocore (Haan et al., 1998) and CFA PLACE CO dataset**
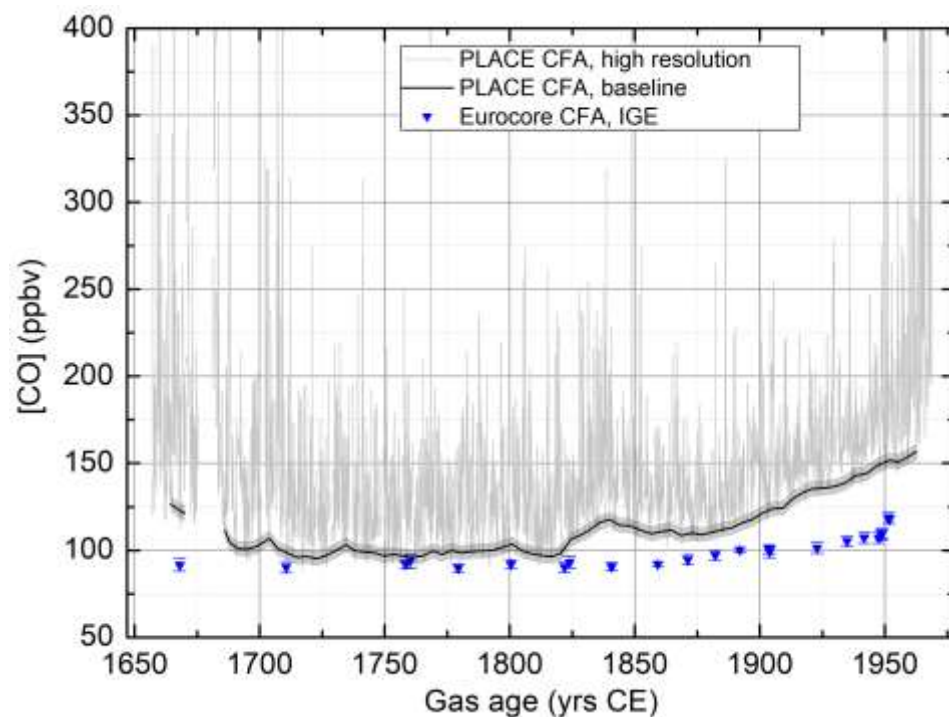
3   **Figure S23.** Continuous CO mixing ratio collected along the Place ice core (grey line) with 5th percentile
4   baseline (black line and envelop), and historical Eurocore discrete CO data (blue dot, Haan et al 1998).

7   **3. Chemistry dataset and analyses**

8   **3.1. High resolution TOC datasets**

9   High resolution, continuous TOC datasets collected at DRI are reported for the PLACE core (Fig.
10   S23) and the Tunu13 core (Fig. S24).

Faïn et al., 2021, CP, Supplementary Information
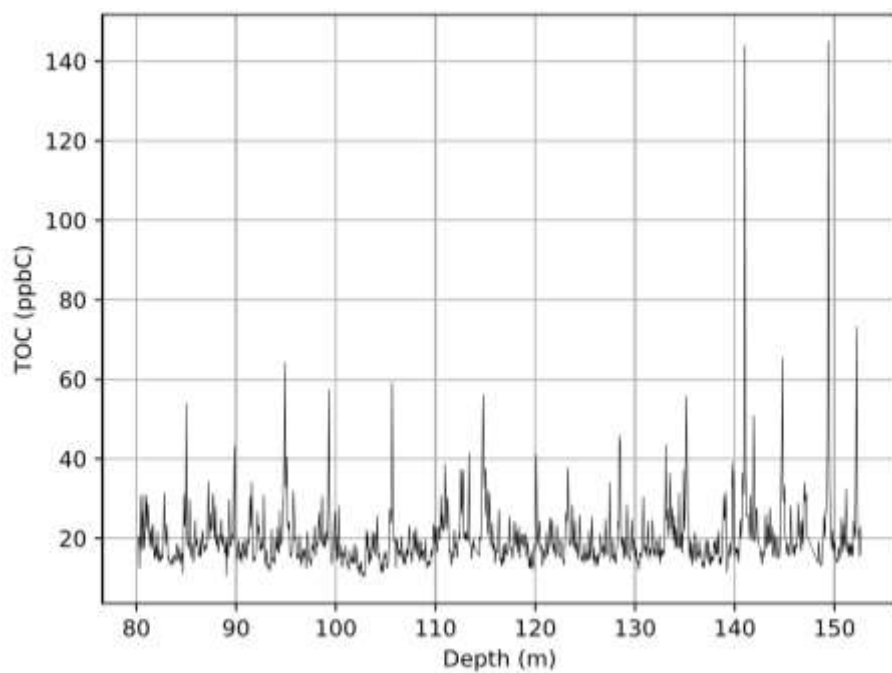
2 **Figure S2~~3~~4.** High resolution, continuous TOC dataset collected along the PLACE core with the DRI CFA

3 setup.

Faïn et al., 2021, CP, Supplementary Information

1   .
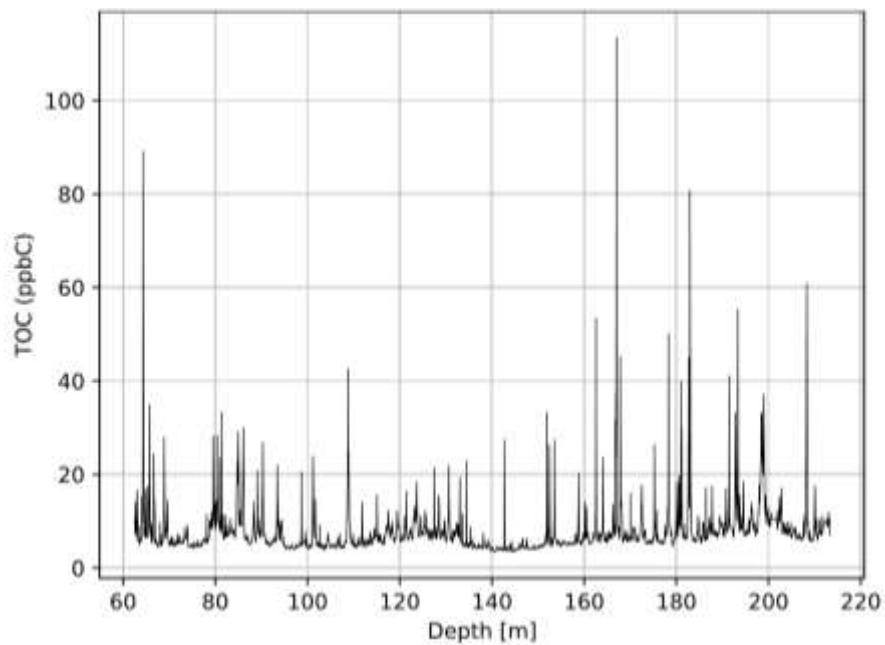
2 **Figure S2~~4~~5.** High resolution, continuous TOC dataset collected along the Tunu13 core with the DRI CFA

3 setup.

| Supprimé: 4 |

Faïn et al., 2021, CP, Supplementary Information

3.2. Seasonal distributions of TOC mixing ratios for the PLACE record

Mis en forme : Centré
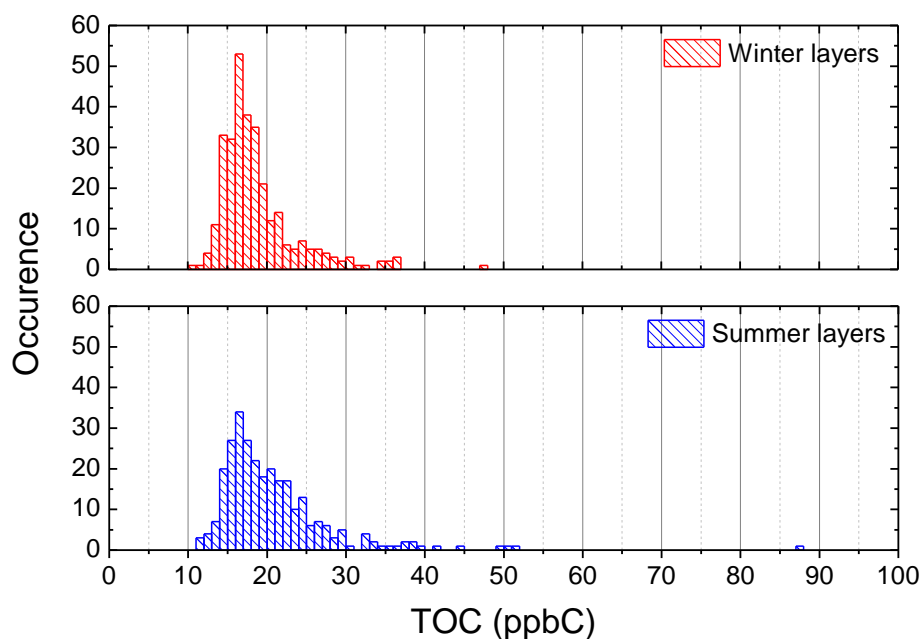
Figure S26. Seasonal distribution of TOC mixing ratios for the full PLACE record. Summer (resp. winter) refers to the 6 months period panning April-September (resp. October-March).

3.3. Relationship between TOC and snow accumulation rate at Tunu13

Figure S26 reports the relationships between TOC and surface snow accumulation rate Tunu13.
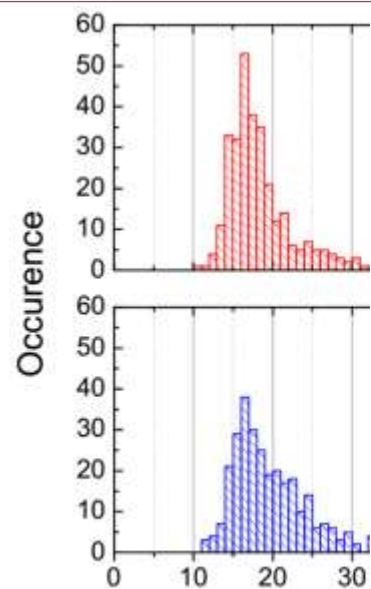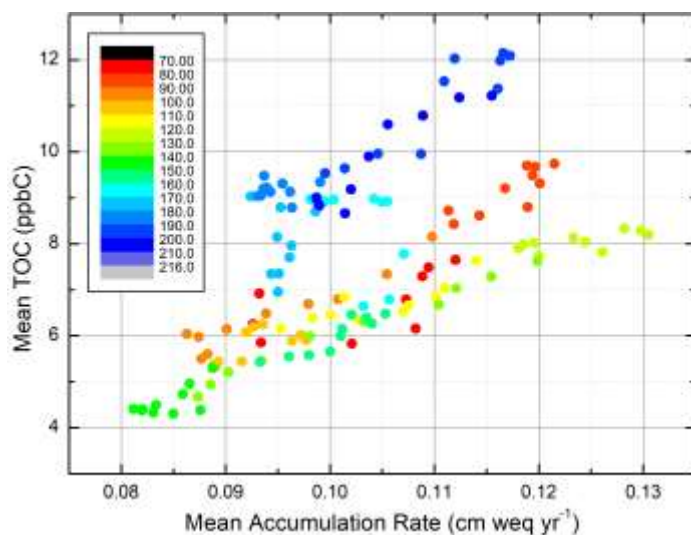
Figure S27. TOC vs Accumulation rate (annually averaged dataset) plotted for the Tunu13 ice core. The color scale reports the depth, varying from 78 to 216 m depth.

3.4. Relationship between TOC and ammonium at Tunu13 and PLACE

Figures S27 and S28 report the relationships between TOC and ammonium at PLACE and Tunu13, respectively.

Faïn et al., 2021, CP, Supplementary Information
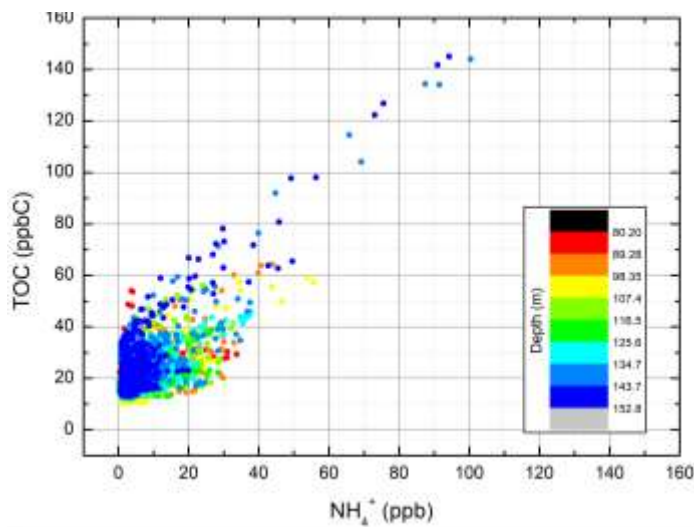
2 **Figure S28.** Relationship between TOC and ammonium for the PLACE ice core. The slope is close to unity.

3 The color scale indicates depth in meters.
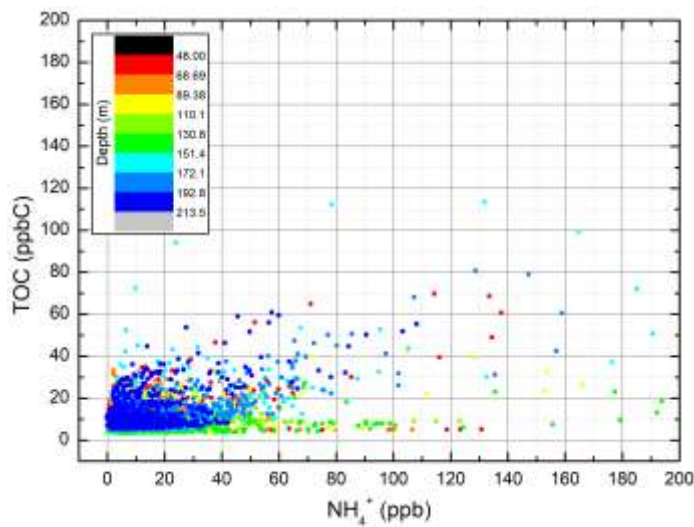
5 **Figure S29.** Relationship between TOC and ammonium for the Tunu13 ice core. Unexpectedly low TOC

6 is observed along ammonium peaks. The color scale indicates depth in meters.

4. References

Allan, D. W.: Statistics of atomic frequency standards, Proc. IEEE, 54(2), 221–230, doi:10.1109/PROC.1966.4634, 1966.

Aydin, M., Montzka, S. A., Battle, M. O., Williams, M. B., De Bruyn, W. J., Butler, J. H., Verhulst, K. R., Tatum, C., Gun, B. K., Plotkin, D. A., Hall, B. D. and Saltzman, E. S.: Post-coring entrapment of modern air in some shallow ice cores collected near the firn-ice transition: evidence from CFC-12 measurements in Antarctic firn air and ice cores, Atmos. Chem. Phys., 10(11), 5135–5144, doi:10.5194/acp-10-5135-2010, 2010.

Bigler, M., Svensson, A., Kettner, E., Vallelonga, P., Nielsen, M. E., Steffensen, J. P. and Peder, J.: Optimization of High-Resolution Continuous Flow Analysis for Transient Climate Signals in Ice Cores, Environ. Sci. Technol., 45(10), 4483–4489, doi:10.1021/es200118j, 2011.

Buizert, C., Martinerie, P., Petrenko, V. V., Severinghaus, J. P., Trudinger, C. M., Witrant, E., Rosen, J. L., Orsi, A. J., Rubino, M., Etheridge, D. M., Steele, L. P., Hogan, C., Laube, J. C., Sturges, W. T., Levchenko, V. A., Smith, A. M., Levin, I., Conway, T. J., Dlugokencky, E. J., Lang, P. M., Kawamura, K., Jenk, T. M., White, J. W. C., Sowers, T., Schwander, J. and Blunier, T.: Corrigendum to "Gas transport in firn: multiple-tracer characterisation and model intercomparison for NEEM, Northern Greenland'" published in Atmos. Chem. Phys., 12, 4259–-4277, 2012", Atmos. Chem. Phys., 14(7), 3571–3572, doi:10.5194/acp-14-3571-2014, 2014.

Faïn, X., Chappellaz, J., Rhodes, R. H., Stowasser, C., Blunier, T., McConnell, J. R., Brook, E. J., Preunkert, S., Legrand, M., Debois, T. and Romanini, D.: High resolution measurements of carbon monoxide along a late Holocene Greenland ice core: evidence for in situ production, Clim. Past, 10(3), 987–1000, doi:10.5194/cp-10-987-2014, 2014.

Fourteau, K., Faïn, X., Martinerie, P., Landais, A., Ekaykin, A. A., Lipenkov, V. Y. and Chappellaz, J.: Analytical constraints on layered gas trapping and smoothing of atmospheric variability in ice under low-accumulation conditions, Clim. Past, 13(12), 1815–1830, doi:10.5194/cp-13-1815-2017, 2017.

Kobashi, T., Severinghaus, J. P., Barnola, J. M., Kawamura, K., Carter, T. and Nakaegawa, T.: Persistent multi-decadal Greenland temperature fluctuation through the last millennium, Clim. Change, doi:10.1007/s10584-009-9689-9, 2010.

MacFarling Meure, C., Etheridge, D. M., Trudinger, C. M., Steele, P., Langenfelds, R., van Ommen, T., Smith, A. and Elkins, J.: Law Dome CO_2, CH_4 and N_2O ice core records extended to 2000 years BP, Geophys. Res. Lett., 33(14), doi:Artn L14810 doi 10.1029/2006gl026152, 2006.

1 McConnell, J. R., Lamorey, S. W. and Taylor, K. C.: Continuous ice-core chemical analyses using

2 inductively coupled plasma mass spectrometry, Environ. Sci. Technol., 36(1), 7–11, 2002.

3 Mitchell, L. E., Brook, E. J., Lee, J. E., Buizert, C. and Sowers, T.: Constraints on the late holocene

4 anthropogenic contribution to the atmospheric methane budget., Science (80)., 342(6161), 964–

5 6, doi:10.1126/science.1238920, 2013.

6 Morville, J., Kassi, S., Chenevier, M. and Romanini, D.: Fast, low-noise, mode-by-mode, cavity-

7 enhanced absorption spectroscopy by diode-laser self-locking, Appl. Phys. B-Lasers Opt., 80(8),

8 1027–1038, doi:10.1007/s00340-005-1828-z, 2005.

9 Rasmussen, S. O., Abbott, P. M., Blunier, T., Bourne, A. J., Brook, E. J., Buchardt, S. L., Buizert,

10 C., Chappellaz, J., Clausen, H. B., Cook, E., Dahl-Jensen, D., Davies, S. M., Guillevic, M.,

11 Kipfstuhl, S., Laepple, T., Seierstad, I. K., Severinghaus, J. P., Steffensen, J. P., Stowasser, C.,

12 Svensson, A., Vallelonga, P., Vinther, B. M., Wilhelms, F. and Winstrup, M.: A first chronology for

13 the North Greenland Eemian Ice Drilling (NEEM) ice core, Clim. Past, 9(6), 2713–2730,

14 doi:10.5194/cp-9-2713-2013, 2013.

15 Rhodes, R. H., Faïn, X., Stowasser, C., Blunier, T., Chappellaz, J., McConnell, J. R., Romanini,

16 D., Mitchell, L. E. and Brook, E. J.: Continuous methane measurements from a late Holocene

17 Greenland ice core: Atmospheric and in-situ signals, Earth Planet. Sci. Lett., 368, 9–19,

18 doi:10.1016/j.epsl.2013.02.034, 2013.

19 Rhodes, R. H., Faïn, X., Brook, E. J., McConnell, J. R., Maselli, O. J., Sigl, M., Edwards, J. S.,

20 Buizert, C., Blunier, T., Chappellaz, J. and Freitag, J.: Local artifacts in ice core methane records

21 caused by layered bubble trapping and in situ production: a multi-site investigation, Clim. Past,

22 12(4), 1061–1077, doi:10.5194/cp-12-1061-2016, 2016.

23 Rosen, J. L., Brook, E. J., Severinghaus, J. P., Blunier, T., Mitchell, L. E., Lee, J. E., Edwards, J.

24 S. and Gkinis, V.: An ice core record of near-synchronous global climate changes at the Bølling

25 transition, Nat. Geosci., 7(6), 459–463, doi:10.1038/ngeo2147, 2014.

26 Sigl, M., Winstrup, M., McConnell, J. R., Welten, K. C., Plunkett, G., Ludlow, F., Büntgen, U.,

27 Caffee, M., Chellman, N., Dahl-Jensen, D., Fischer, H., Kipfstuhl, S., Kostick, C., Maselli, O. J.,

28 Mekhaldi, F., Mulvaney, R., Muscheler, R., Pasteris, D. R.,Stowasser, C., Buizert, C., Gkinis, V.,

29 Chappellaz, J., Schüpbach, S., Bigler, M., Faïn, X., Sperlich, P., Baumgartner, M., Schilt, a.,

30 Blunier, T. and Schupbach, S.: Continuous measurements of methane mixing ratios from ice

31 cores, Atmos. Meas. Tech., 5(5), 999–1013, doi:10.5194/amt-5-999-2012, 2012.

Faïn et al., 2021, CP, Supplementary Information

1   Stowasser, C., Buizert, C., Gkinis, V., Chappellaz, J., Schüpbach, S., Bigler, M., Faïn, X., Sperlich,

2   P., Baumgartner, M., Schilt, a., Blunier, T. and Schupbach, S.: Continuous measurements of

3   methane mixing ratios from ice cores, Atmos. Meas. Tech., 5(5), 999–1013, doi:10.5194/amt-5-

4   999-2012, 2012.